

Chapter 1

High-Power Single-Frequency Fiber Amplifiers

Chun-Wei Chen

Department of Physics, University of Bath, Bath BA2 7AY, UK
Department of Applied Physics, Yale University, New Haven, CT, USA
Edward L. Ginzton Laboratory, Stanford University, Stanford, CA, USA
For correspondence: cwc218@bath.ac.uk

High-power single-frequency fiber amplifiers are increasingly dominant in technologies that require high optical power, stability, and coherence simultaneously. In this chapter, we first provide an overview of their key characteristics, applications, architectures, and components. We then review the nonlinear acousto- and thermo-optical instabilities that limit power scaling and summarize the primary mitigation techniques. Finally, we discuss multimode excitation with wavefront shaping and anti-Stokes fluorescence cooling as two emerging strategies to circumvent the limitations of current approaches.

1. Introduction

Fiber lasers bring together compactness, high efficiency, low cost, and superior thermal management, making them a compelling and increasingly dominant light source across diverse technologies, from optical communications¹ and materials processing^{2,3} to remote sensing,^{4–6} directed energy,^{7–9} and space photonics.^{10–12} Many of these applications demand laser powers ranging from watts (W) to kilowatts (kW) or higher. To produce high-power output while maintaining diffraction-limited performance (with a beam quality factor of $M^2 \approx 1$) and the desired optical properties, a master-oscillator power-amplifier (MOPA) comprising double-clad active fibers has so far proven to be one of the most effective architectures.^{13–18} (Note: M^2 is defined as the product of a beam's width and divergence angle relative to that of an ideal Gaussian beam.)

Among the various laser types achievable with MOPA, this chapter fo-

cuses on high-power single-frequency fiber amplifiers, which are in high demand for technologies that require high coherence, stability, and/or spectral purity at elevated power levels.^{19,20} Key applications include directed energy, coherent lidar, and gravitational-wave detection. The ideal concept of a “single-frequency” source outputs *monochromatic* light, meaning zero spectral linewidth, absence of phase and frequency noise,²¹ and infinitely high coherence. However, as no real-world laser is truly monochromatic, the term practically refers to lasers with an extremely narrow linewidth, typically below one megahertz (MHz). A linewidth of 1 MHz in frequency is equivalent to several femtometers (fm) in wavelength in the near-infrared regime (with a center wavelength around 1–2 μ m) and corresponds to a longitudinal (temporal) coherence length L_c on the order of 100 meters.

Compared to bulk gain media (e.g., laser crystals), fiber amplifiers benefit from light guiding, which provides excellent beam quality, a long gain length for high pump efficiency, and a large surface-area-to-volume ratio for effective heat dissipation. However, concentrating so much power in a small core (\sim 10 μ m in diameter) yields significantly high intensity, readily triggering nonlinear optical effects that limit power scaling of fiber lasers. In single-frequency fiber amplifiers, the nonlinear effects with the lowest thresholds are stimulated Brillouin scattering (SBS) and transverse mode instability (TMI).^{22–24} SBS is the nonlinear backscattering of light by sound waves induced by optical forces,²⁵ while TMI is the thermo-optically induced dynamic coupling between the fundamental and higher-order transverse modes.²⁶ Consequently, recent advancements in single-frequency fiber amplifiers have focused on mitigating these nonlinear effects to push the maximum output power, which currently stands at 1.0 kW [Fig. 1].²⁷

1.1. *Linewidth and power needed*

Here, we outline the power and linewidth requirements for three example applications of high-power single-frequency fiber amplifiers.

Directed energy. Delivering a laser beam with sufficiently high power (0.1–1 MW) to a small distant target often requires the coherent combination of multiple laser beams through optical interference, ensuring their powers add up constructively within the target spot.^{8,9,28,29} The laser linewidth $\Delta\nu_s$ determines the longitudinal coherence length L_c , which defines the distance over which multiple laser beams can interfere with each other. $L_c = Fc/(n\Delta\nu_s)$, where F is a prefactor that depends on the lineshape,³⁰ c is the speed of light in vacuum, and n is the refractive in-

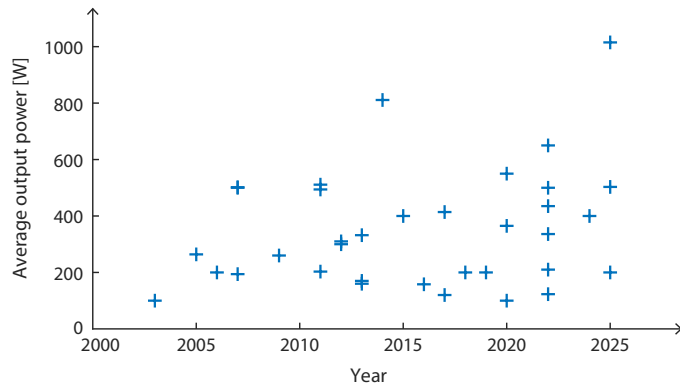


Fig. 1. Power scaling of single-frequency fiber amplifiers. Overview of average output powers reported for single-frequency Yb-doped fiber amplifiers over the past 15 years. All data points exceed 100 W and are taken from publications cited herein.

dex. When the coherence length is short, the optical path lengths of the laser beams must be matched with high precision. Balancing power and linewidth requirements, the linewidth of most fiber lasers used in directed energy is on the order of 1–10 GHz ($L_c \sim 1$ –10 cm) at kilowatts.^{9,31–33}

Coherent lidar. An object’s distance and motion can be measured by interfering the backscattered signal from the object with a reference signal from the local oscillator (optical heterodyne detection).^{4–6} The coherence length, which is inversely proportional to the laser linewidth, places a strong constraint on the maximum detectable range.^{34,35} Since the intensity of the backscattered signal decreases rapidly with propagation distance, this range is also limited by the laser power determining how much light is available to maintain a sufficient signal-to-noise ratio (SNR). For continuous-wave lidar, kilometer-scale detection typically requires laser powers on the order of 0.1–10 W and linewidths of about 10–100 kHz.^{4,34,35} Furthermore, a moving object’s velocity is obtained from the Doppler shift of the backscattered signal relative to the local oscillator frequency, so the laser linewidth determines the minimum resolvable frequency shift and therefore the lowest measurable velocity. For example, a 100-kHz laser can detect objects moving as slowly as \sim 10 cm/s.³⁴ As detection ranges continue to increase, lasers with narrower linewidths and higher output powers are required. A particularly demanding application is ground-based, high-resolution imaging of space objects at distances of \sim 100 km to \sim 100,000 km (toward the Moon and possibly beyond).¹² In this context, the terms *ladar* and

laser radar are commonly used to emphasize the functional parallels with radio-frequency or microwave radars.³⁶ Such applications may require laser linewidths down to the hertz level and output powers reaching 100 kW or higher.¹²

Gravitational-wave detection. These detectors are Michelson interferometers with each arms being a 3–4-km-long Fabry–Perot cavity,³⁷ which effectively increase the optical path length and power. They require lasers with exceptionally high coherence to resolve mirror displacements far smaller than the width of a proton, and even small amounts of laser phase noise can obscure the true gravitational-wave signal.^{38–40} Therefore, extremely high phase stability is needed, demanding a laser with an intrinsic kHz linewidth, which is then actively stabilized to achieve a linewidth of 0.1–1 Hz.^{41–50} To reach the required signal-to-noise ratio, the injected laser power is \sim 10–100 W with ultralow power noise, which is then built up to nearly 1 MW circulating in the arm cavities.^{38–40,51} For such long cavities, high beam quality and pointing stability are also critical to enable efficient power recycling and precise mode matching.^{40,41}

1.2. *Master-oscillator power-amplifier (MOPA)*

MOPA⁵² begins with a seed laser (the master oscillator) that generates an optical signal with desired spectral and temporal properties but at relatively low power (up to \sim 0.1 W) [Fig. 2(a,b)]. This signal first passes through an optical isolator, which protects the source from linear and nonlinear backscattering that could otherwise destabilize or damage the seed laser. The signal then enters a pump–signal combiner, where it is combined with pump light and launched into a rare-earth-doped fiber (the power amplifier). The pump light excites the rare-earth ions, and the signal photons then trigger these excited ions to release identical photons in a chain of stimulated-emission events, thereby amplifying the signal power. The active fiber’s output end (where the amplified signal enters free space) is usually angle-cleaved by $\gtrsim 4^\circ$ or end-capped to minimize the back-reflection of both the signal and amplified spontaneous emission (ASE) into the doped core.^{53–57} This prevents strong (re-amplified) backward signal and parasitic lasing (self-lasing), both of which could damage upstream components. While angled cleaving is suitable for powers up to a few tens of watts, end-capping is generally required to handle higher powers.

Minimizing unwanted light is crucial throughout the fiber amplifier, not just at the output. Cladding-light strippers are often integrated within the

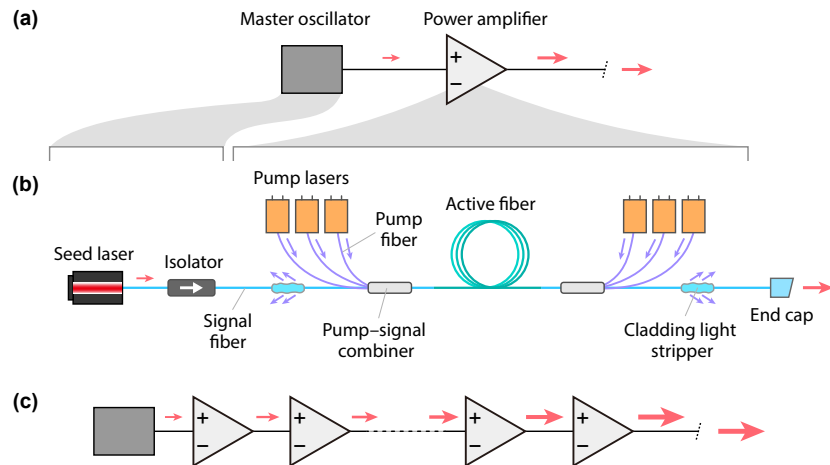


Fig. 2. **Master-oscillator power-amplifier (MOPA).** (a) Conceptual illustration, where a laser signal generated by the master oscillator is amplified by a power amplifier. (b) Fiber-based implementation. (c) Cascaded amplifier stages for power scaling.

amplifier on the side opposite the pump combiners, as well as between the pump lasers and combiners.^{57–60} They are implemented by first stripping a section of the fiber, then either coating the bare cladding with a higher-index epoxy^{59,61} or roughening the cladding surface.^{58,60} The strippers remove residual pump light to avoid thermal damage to surrounding components and free-space optics, and prevent backscattered signal and ASE from re-entering the core and becoming re-amplified.

To effectively suppress ASE in a high-power fiber amplifier, a key strategy is to saturate the optical gain with sufficiently strong seed signal. When the initial seed power is low, it is common to cascade power amplifiers to ensure gain saturation throughout the system [Fig. 2(c)]. Gain saturation also suppresses the relative intensity noise (RIN) transferred from the seed laser to the output signal^{62,63} and transverse mode instability (see Sec. 3.3). To enhance ASE suppression, tilted fiber Bragg gratings can be spliced to the active fibers to couple them out of the core.^{57,64,65}

Effective thermal management of all MOPA components is essential for stable operation and to prevent damage.^{66–79} For output powers above a few tens of watts, active cooling using liquid-cooled metal baseplates is often required.^{69,71,74}

1.3. Double-clad fiber

A *single-clad* single-mode fiber amplifier produces diffraction-limited signal output (below the nonlinear instability thresholds), making it attractive for many applications. However, efficient coupling of the pump light into the core requires a single-mode pump laser, whose output power is typically limited to \sim 100 mW. To use pump lasers with much higher power, the fiber core can be enlarged, but this introduces higher-order modes. As a result, the signal output often becomes speckled, leading to poor beam quality.

Double-clad fibers were pioneered by Snitzer *et al.* to decouple the core size for pump light from that for signal light.^{80,81} These fibers consist of a rare-earth-doped single-mode core surrounded by two undoped claddings, with the highest refractive index in the core and the lowest in the outer cladding [Fig. 3(a)]. In a double-clad fiber amplifier, the signal is coupled into the core and the pump light into the inner cladding. This ensures that the signal stays confined within the doped core, while the pump light propagates through a *larger core*, formed by the inner cladding and doped core. The central portion of the pump light overlaps with the core and is thus absorbed. Since the numerical aperture (NA) and size of the inner cladding can be much greater than that of the core, it becomes possible to efficiently couple substantial pump power from low-brightness sources, such as multimode (single-emitter) or multi-emitter diode lasers. In a multimode laser, all spatial modes that lase do so independently, causing their intensity profiles to superimpose incoherently in space. As a result, the intensity distribution of the pump beam becomes nearly uniform across the inner cladding and doped core. The same applies to multi-emitter lasers, where all emitters lase independently. The absorption coefficient of a cladding-pumped fiber is lower than in the core-pumped case and scales roughly with the core-to-cladding area ratio.

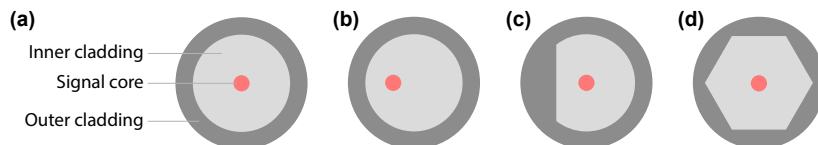


Fig. 3. Common cross-sectional geometries of double-clad fibers. (a) Centered core, (b) off-centered core, (c) D-shaped inner cladding, and (d) hexagonal inner cladding.

The shape of the inner cladding is critical for maximizing pump absorption efficiency [Fig. 3]. The simplest design, featuring circular symmetry for all three layers (core, inner cladding, and outer cladding) centered on the fiber axis, is straightforward to fabricate and facilitates pump light coupling. However, this structure supports many higher-order pump modes that have almost no power overlap with the core and thus unabsorbed.^{82–84} Significant pump power is wasted. One approach to enhance pump absorption is to induce mode scrambling through bending, twisting, or squeezing the fiber.⁸⁵ For instance, kidney-shaped coiling has proven effective.^{85–87} Nevertheless, the fibers for high-power amplifiers typically have large outer diameters, making them more rigid and thus challenging to manipulate mechanically. A more effective approach is to break the circular symmetry. One way to do this is by shifting the doped core off-center, which allows more modes to overlap with it.^{80,81,88} Non-circular inner claddings also enhance pump absorption by forcing the pump modes to extend across almost the entire cross-section, particularly the chaotic ones like D (circular with a straight cut) or stadium shapes.^{17,82–84,86,88–90} However, irregular shapes pose challenges in launching pump light with low insertion loss, so relatively symmetric shapes, like hexagon or octagon, are more widely used.^{84–87,91}

1.4. Core composition

Fiber amplifiers are primarily based on glass fibers doped with rare-earth ions in the core, such as Yb^{3+} , Er^{3+} , Tm^{3+} , Ho^{3+} , Nd^{3+} , Pr^{3+} , Dy^{3+} , Sm^{3+} , and Tb^{3+} .^{13,57,91–94} Under optical pumping, these ions absorb pump light and are excited from their ground state to a higher energy state. They then relax to lower energy states, emitting light with photon energy lower than the pump through either spontaneous emission (fluorescence) or stimulated emission (signal amplification). Ytterbium (Yb^{3+}) is commonly used for amplification in the 1.0 μm region,⁹⁵ erbium (Er^{3+}) for the 1.5 μm region,⁹⁶ and thulium (Tm^{3+}) for the 2.0 μm region.^{97,98} If a primary rare-earth dopant is chosen for its emission spectrum but suffers from weak pump absorption, it is often co-doped with another rare-earth element that has strong pump absorption and facilitates efficient energy transfer to the primary dopant.^{99,100} For example, Er^{3+} is often co-doped with Yb^{3+} to enhance pump absorption per unit length, enabling more efficient amplification in the telecom band.¹⁰¹

The host glass composition is similarly critical. It determines the fiber's core refractive index^{102,103} and spectral transparency window,^{100,104}

modifies the spectroscopic properties of the rare-earth ions (e.g., emission/absorption cross-sections, spectral shapes, and transition lifetimes),¹⁰⁵ limits the maximum doping concentration (due to quenching),¹⁰⁵ and affects other factors relevant to laser performance, such as resistivity to photodarkening,¹⁰⁶ optical nonlinearities,^{107–111} and high-energy radiation.¹¹² Silicates are the most widely used host glass in fibers due to their exceptional transparency in the visible and near-infrared regions, mechanical strength, chemical stability, and mature fabrication techniques.¹¹³ Pure silica (SiO_2) exhibits poor solubility for rare-earth ions, requiring the use of co-dopants, such as aluminum (Al) and phosphorus (P), to reduce ion clustering and resulting quenching.¹¹⁴ Co-dopants can also be used to modify other properties, such as using cerium (Ce) or sodium (Na) to mitigate photodarkening.^{106,115} Beyond the initial host composition, the processes of preform fabrication and subsequent fiber drawing can significantly influence the compositional profiles across the core and, consequently, the properties mentioned above.^{116,117}

1.5. Seed laser

To ensure the linewidth is sufficiently narrow to be considered single-frequency (typically on the order of 1 MHz or below), the seed laser produces a low-noise continuous-wave (CW) signal or pulses longer than ~ 100 ns, with a time–bandwidth product close to the Fourier transform limit. Typical sources include diode lasers with distributed feedback (DFB), distributed Bragg reflector (DBR), or external-cavity configurations,^{118–120} fiber lasers using DFB, DBR, or ring cavities,^{19,121–128} and nonplanar ring oscillators (NPROs) based on shaped laser crystals.^{39,42,129} The selection of the seed laser generally depends on the required wavelength, spectral purity, amplitude and phase noise spectra, modulation capability, and output power, which can vary substantially with the specific application or experimental requirements. For Yb-doped fiber amplifiers, 1064 nm is the standard seed wavelength, with several studies targeting operation at 1030 and 1080 nm [Fig. 4].^{27,61,130–132}

These sources tend to be low power for architectural reasons. For instance, in a DFB fiber laser, a Bragg grating written in the active fiber incorporates a π -phase shift at its center to create a single ultranarrow resonance at the center of the photonic bandgap. The effective gain length is consequently very short, limiting the maximum output power to ~ 100 mW.¹²⁶ In DBR fiber lasers (comprising two Bragg gratings sandwiching an active

fiber), the cavity must be short enough to support only one longitudinal mode, yet relatively long (~ 1 cm) to enable higher power (~ 1 W).¹²⁵ Ring-cavity fiber lasers can employ meter-scale gain lengths and incorporate sub-cavities or saturable absorbers to enforce single-longitudinal-mode operation.¹²⁷ Their output can exceed that of the previous two types, but typically remains at the watt level.

For oscillators with adjustable laser frequency, the linewidth can be pushed to the hertz or sub-hertz regime through self-injection locking or Pound–Drever–Hall (PDH) locking to a reference cavity with an ultrahigh quality factor.^{133–140} Preserving the linewidth at this level through a high-power fiber amplifier has not yet been demonstrated and can be challenging, as additional noise can be introduced in the amplification stages.

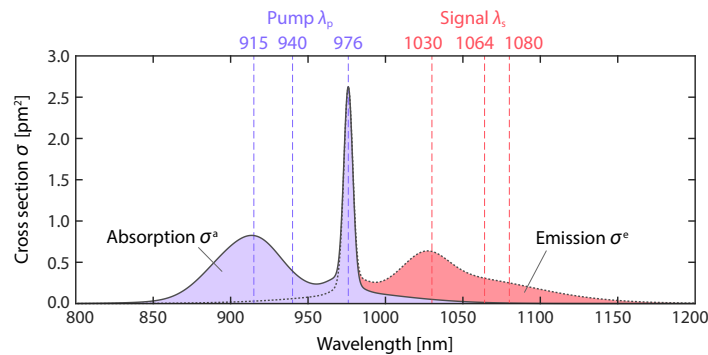


Fig. 4. **Absorption and emission spectra of Yb-doped silicate fiber.** Solid and dotted curves are example spectra of absorption cross-section (σ^a) and emission cross-section (σ^e), respectively. Dashed lines mark the common pump wavelengths (λ_p) and signal wavelengths (λ_s). Spectra were generated using open-source codes developed by Luke Rumbaugh.¹⁴¹

1.6. Pump laser

Fiber amplifiers are commonly pumped by fiber-coupled diode lasers.^{142–144} These diode lasers can be single emitters or one-dimensional emitter arrays (laser bars), selected according to the required power, brightness, and coupling configuration. When pumping the core directly, diffraction-limited single-mode diodes are needed to couple the pump light efficiently into a single-mode active fiber, but their average output powers are relatively low (typically ~ 1 –100 mW).

To achieve higher power output, multimode pump diodes, such as broad-area chips or laser bars, are the most practical option.^{142–144} However, the presence of higher-order modes results in both a large beam size and increased divergence. This challenge is overcome through the use of double-clad active fibers, which allow the pump light to be efficiently coupled into a large inner cladding with high NA, as discussed earlier in Sec. 1.3.

High-power pump modules typically deliver \sim 0.1–1 kW of power, with wall-plug (electrical-to-optical) efficiencies around 50–80%.^{145,146} The power loss turns into heat, which often requires active dissipation through liquid-cooled metal plates (cold plates) or thermoelectric coolers (TEC). Heating also shifts the pump wavelength by \sim 0.1–1 nm/W.^{147,148} This can be addressed through active temperature control or passive wavelength stabilization by coupling the diode laser to a volume Bragg grating or fiber Bragg grating (\sim 10% reflectivity, \sim 0.1–1-nm bandwidth). Alternatively, pumping within a broad flat absorption band can reduce sensitivity to wavelength drift. For example, in Yb-doped fiber lasers and amplifiers, it is common to pump around 915 or 940 nm instead of 976 nm (with maximum absorption but spectrally narrow) [Fig. 4].^{149,150}

To reduce quantum-defect heating in a fiber amplifier and improve its slope efficiency by pumping closer to the signal wavelength, some systems use fiber lasers as pumps when high-power diodes are unavailable at the desired wavelength.^{15,151–153} This approach is known as tandem pumping. Examples include pumping a 2.09- μ m Ho-doped fiber amplifier with a 1.95- μ m Tm-doped fiber laser,¹⁵³ pumping a 1.55- μ m Er-doped fiber amplifier with a 1.48- μ m Raman fiber laser,¹⁵⁴ and pumping a 1.56- μ m Er/Yb-codoped fiber amplifier with a 1.02- μ m Yb-doped fiber laser.¹⁵⁵

1.7. Pump–signal combiner

A pump–signal combiner is the component that couples pump light into the active fiber, either in an all-fiber configuration or via free-space optics.^{156,157} It may be placed at the fiber input (co-pumping), at the output (counter-pumping), at both ends (bidirectional), or mid-span along the active fiber to extend the effective gain length (distributed pumping) [Fig. 2(b)].^{17,62,68,158}

In all-fiber configurations, pump light can be coupled from either the fiber end or the side [Fig. 5(a,b)]. End-pumping employs a multi-port combiner: several pump fibers surround a central signal fiber to form a bundle, which is then tapered and fusion-spliced to a passive double-clad fiber matched in geometry and NA to the active fiber [Fig. 5(a)].^{159–161}

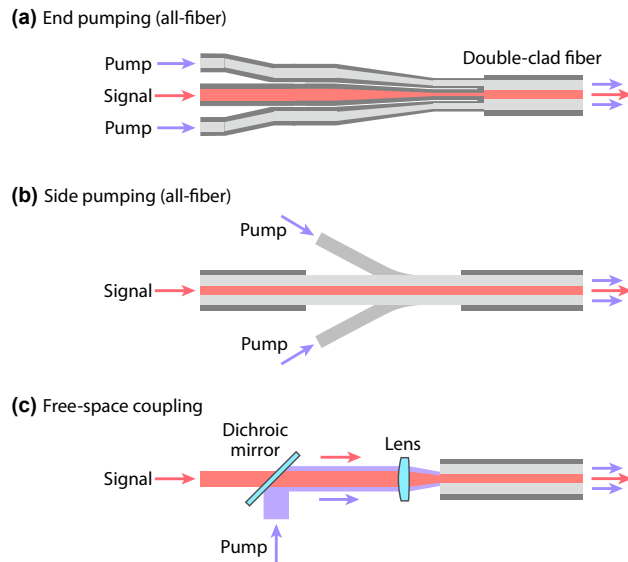


Fig. 5. **Pump–signal combiners.** (a) All-fiber end pumping, (b) all-fiber side pumping, and (c) free-space coupling using dichroic mirror and lens.

Local tapering in this arrangement alters the signal-core diameter along the combiner, potentially degrading performance in certain applications. End-pump combiners can also be built for core-pumping a single-clad active fiber, but this requires single-mode pump fibers, and the small core of the output fiber limits the number of pump inputs.^{154,162}

In side-pump combiners, a section of the matching passive fiber's outer cladding is removed, and pump fibers are spliced to a bridging structure (e.g., tapered coreless fibers) attached to the stripped matching fiber to couple light at an angle into the inner cladding [Fig. 5(b)].^{159,163–165} They support co-, counter-, and distributed pumping and maintain a constant signal-core diameter throughout the device.

As all-fiber combiners may contain several splice points through which high pump power is injected, scattering of the pump light can occur at these interfaces. Subsequent absorption of this stray light causes significant heating, making efficient heat dissipation essential to prevent damage.⁷¹ With appropriate combiner design and thermal management, they can handle multi-kilowatt power.^{166,167} It's also worth noting that, if no matching passive fiber is available, the active fiber can be integrated directly with

the combiner. However, substantial pump absorption and the ensuing heat load limit the power-handling capability of active pump–signal combiners compared with passive ones.

Free-space coupling is often used when the active fiber uses a custom geometry or NA for which all-fiber combiners are unavailable [Fig. 5(c)].^{62,168–171} For co-pumping in free space, the pump and signal are combined onto a common optical path with a dichroic mirror and then focused by a lens into the input end of the active fiber. Counter-pumping uses the same optics in a mirrored arrangement at the output end. Implementing distributed pumping with free-space optics is generally impractical (alignment-sensitive), bulkier, and offering little benefit compared with all-fiber solutions.

2. Mitigation of Stimulated Brillouin Scattering (SBS)

2.1. What is SBS?

Stimulated Brillouin scattering (SBS) is a nonlinear interaction between light and acoustic waves.^{25,172,173} In an optical fiber, thermally excited acoustic waves are always present and can scatter the signal light, generating Stokes-shifted light. This spontaneous Brillouin scattering provides the initial Stokes seed for the SBS process. The efficiency of SBS is governed by the phase-matching condition, which is most readily satisfied for counter-propagating optical waves coupled through a guided acoustic wave: $q = \beta_s - \beta_{St} \approx 2\beta_s$, where q , β_s , and β_{St} are the propagation constants for the acoustic, signal, and Stokes waves, respectively. This Stokes wave propagates in the backward direction and has a slightly lower frequency of $\omega_{St} = \omega_s - \Omega$, where ω_s and $\Omega = 2\pi\nu$ are the signal and acoustic frequencies, respectively. The interference between the signal and Stokes waves forms a traveling intensity grating with velocity Ω/q , which in turn drives the guided acoustic wave through electrostriction. The acoustic wave then scatters more signal power into the Stokes, triggering a stimulated process. As a result, the Stokes field grows exponentially in the backward direction along the fiber [Fig. 6(a)].

SBS is the primary nonlinear effect limiting the power-scaling of single-frequency fiber amplifiers for two main reasons. Both stem from the characteristics of the *Brillouin gain spectrum* $g_B(\Omega)$, which determines the exponential growth rate of the Stokes field [Fig. 6(b)].

First, this spectrum is very narrow. In silicate fibers, acoustic waves

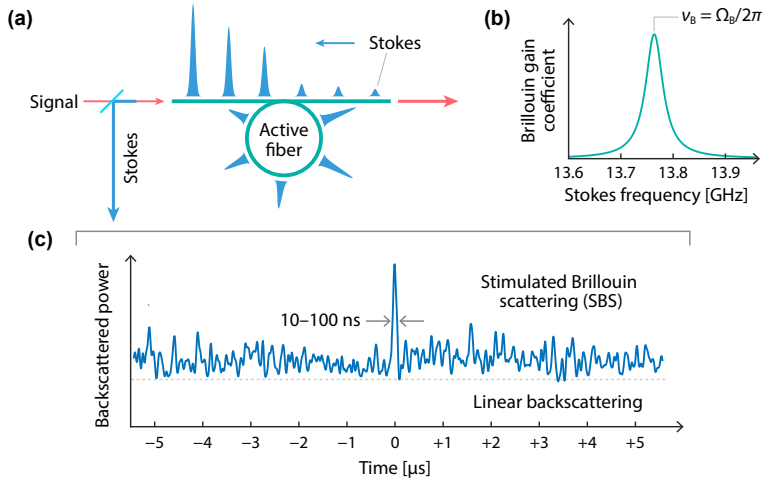


Fig. 6. **Stimulated Brillouin scattering (SBS) in fiber amplifier.** (a) Backward-propagating Stokes field gains power from the forward signal via SBS and from stimulated emission. (b) Typical Brillouin gain spectrum $g_B(\nu)$ in single-mode silicate fibers, centered at $\nu_B = \Omega_B/2\pi \approx 10\text{--}20$ GHz from the signal frequency. The Stokes shift is expressed in linear frequency ν to follow experimental literature conventions. Data were generated using open-source codes developed by Wisal *et al.*¹⁷⁴ (c) Example time trace of backscattered power near the onset of SBS (synthetic data),^{23,175} showing amplified Stokes fluctuations with intermittent strong pulses (10–100-ns duration) on top of constant linear backscattering from Fresnel reflection and Rayleigh scattering.

decay exponentially as $\exp(-t/\Gamma_B)$, where the phonon decay rate Γ_B is typically on the order of 10–100 MHz. This decay rate determines the Brillouin gain bandwidth $\Delta\nu_B = \Gamma_B/2\pi$, which falls within the same frequency range.^{172,176,177} Because the linewidth of single-frequency lasers ($\lesssim 1$ MHz) is well below this gain bandwidth, virtually all frequency components of the laser light contribute coherently to the SBS process. As a result, the laser power is efficiently transferred into the backward Stokes field.

Second, the peak frequency is very low. The Brillouin gain spectrum is peaked at frequency $\Omega_B = qV_a$, where V_a is the longitudinal acoustic velocity in glass. Using the phase-matching condition $q \approx 2\beta_s$, this frequency can then be written as $\Omega_B = 2\beta_s V_a = 4\pi n V_a / \lambda_s$, where n is the refractive index and λ_s is the signal wavelength in vacuum. For silicate fibers operating in the near-infrared, the resulting Stokes shift ν_B (often preferred in experimental contexts, where $\nu_B = \Omega_B/2\pi$) is only about 10 to 20 GHz, which is less than 100 pm in wavelength.^{25,111,172} Consequently, the Stokes field remains well within the gain bandwidth of the rare-earth

dopants, allowing it to draw energy not only through SBS but also from the population inversion. This causes the Stokes power to grow more aggressively than in passive fibers, potentially leading to catastrophic damage to upstream components.

SBS in fiber amplifiers is commonly characterized by measuring the backscattered power (as a time trace or a time-averaged value) at the fiber input against the pump power [Fig. 6(c)].²³ At low pump powers, the backscattered Stokes field first appears as random noise fluctuating on the 10–100-ns scale (associated with the phonon lifetime $\tau_B = 1/\Gamma_B$).¹⁷² With increasing pump power, the Stokes fluctuations are amplified, leading to the emergence of intermittent high-power pulsing with 10–100-ms intervals. The interval shortens as the pump power continues to rise, eventually evolving into quasi-periodic pulsing. At higher pump powers, occasional giant pulses with kW-level peak power can occur, depleting most of the available optical gain and followed by a 10-μs-scaled gain recovery. For safe and stable amplifier operation, the pump power should be limited below the onset of quasi-periodic pulsing. Even if no physical damage occurs, the strong noise added by SBS can severely degrade signal coherence.

Because the Stokes power generally increases exponentially with pump power, there is no strict SBS threshold. In amplifiers especially, deleterious effects from intense Stokes pulses may arise even when the average backscattered power is still too low to measurably affect the linear scaling of output power with pump power. Therefore, different studies use varying practical definitions, such as the ratio of average backscattered power to output signal power (e.g., 0.1%),^{102,178} the peak backscattered power relative to the background,¹⁷⁵ or the relative intensity noise at the output.^{47,62,179} This makes direct comparison between published results challenging. Nevertheless, regardless of the definition used, the SBS threshold P_{SBS} scales proportionally with the effective mode area A_{eff} , and inversely with the effective Brillouin gain coefficient coefficient $g_{B,\text{eff}}$ and the effective fiber length $L_{\text{eff}} = \int_0^L P_s(z)/P_s(L) dz$ (accounting for the variation in signal power along the amplifier):

$$P_{SBS} \propto \frac{A_{\text{eff}}}{g_{B,\text{eff}} L_{\text{eff}}}. \quad (1)$$

Single-frequency fiber amplifiers are typically designed with the shortest possible length to suppress SBS, so we won't delve into the length effect or related methods in the following subsections. However, it's worth noting that some studies use high rare-earth doping to significantly reduce the required active length.¹⁸⁰ While SBS is greatly suppressed, this high gain

can lead to intense localized heating, which carries the risk of triggering unwanted thermal effects or even damaging the fiber.

2.2. Intensity reduction with a larger core size

Increasing the core area A_{core} leads to a larger effective mode area A_{eff} , thus suppressing SBS by reducing the intensity for a given power. However, a large core typically supports higher-order modes, whose interference produces a speckled output beam.²⁵ Therefore, various fiber designs have been developed to increase the core size while maintaining single-mode operation ($V < 2.405$) to preserve beam quality. Here $V = 2\pi a \text{NA}/\lambda_s$, where a is the core radius, NA is the numerical aperture, and λ_s is the signal wavelength.

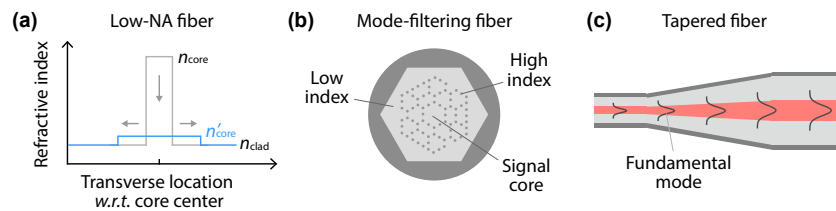


Fig. 7. **Large-core fiber designs for single-mode operation.** (a) Refractive-index profiles of low-NA versus standard step-index fiber. (b) Cross section of mode-filtering photonic crystal fiber.¹⁸¹ (c) Tapered fiber for selective excitation of the fundamental mode in a multimode core through adiabatic core expansion.

Low NA. One common approach is to reduce the NA of the core to counterbalance the increase in core area ($A_{\text{core}} = \pi a^2$), since the number of modes per polarization in a step-index fiber is roughly $V^2/4 = \pi A_{\text{core}} \text{NA}^2/\lambda_s^2$ [Fig. 7(a)].^{61,130,168,180,182–184} This is achieved by carefully adjusting the glass composition^{102,103} so that the core refractive index is brought exceptionally close to that of the cladding. Currently, the minimum achievable NA is ≈ 0.03 , which supports single-mode core diameters up to around 30 μm .²⁷ Fabrication of these fibers is challenging because achieving such a low NA requires the core–cladding index difference to be on the order of 10^{-4} with high transverse and longitudinal uniformity. This demands high-precision control over dopant distributions throughout preform and fiber-drawing stages. Moreover, the fundamental mode is only weakly confined, so the fiber should be kept straight or coiled with a large diameter to minimize bend loss.

Mode filtering. Another route is to employ mode-filtering fiber designs, including photonic crystals,^{169,181,185–188} chirally coupled cores,^{47,179,189} leaky channels,¹⁹⁰ and anti-resonances¹⁹¹ [Fig. 7(b)]. In these fibers, the cladding structure is engineered so that higher order modes in the core are resonant with cladding modes and are thus preferentially stripped away. Similar to low-NA fibers, these microstructured designs are also susceptible to bending, as tight coiling can induce unwanted power transfer from the low-loss fundamental mode to high-loss higher order modes. In addition to structural mode-filtering, the gain profile can also be tailored to minimize its overlap with higher order modes and consequently suppress their growth.^{192–195} This approach is known as confined doping.

A new record for the highest output power in single-frequency fiber amplifiers was recently established (August 2025), reaching 1,015 W, using a large-core fiber with a bat-shaped index profile.²⁷

Taper. To overcome the core size limit imposed by the single-mode condition in step-index fibers ($V < 2.405$), *tapered* fibers have been explored for high-power single-frequency amplifiers, reaching up to 650 W.^{131,149,196,197} These tapered fibers begin with a small-core section for signal input, adiabatically taper to a large core, and end with a uniform large-core section [Fig. 7(c)]. In the front section, only the fundamental mode is excited due to the single-mode core. As the signal propagates through the taper, the fundamental mode area gradually expands. A tapered fiber suppresses SBS through two effects: (1) The intensity remains low throughout the fiber as the signal reaches its maximum power in the large-core section. (2) The frequency of the peak Brillouin gain (known as the Brillouin frequency ν_B) shifts with the fiber diameter. This leads to an effective broadening of the Brillouin gain spectrum (increasing $\Delta\nu_{B,\text{eff}}$), which in turn reduces its peak value.¹⁹⁸ This approach allows for the use of a much larger core diameter, up to around 60 μm , with the SBS threshold typically in the kilowatt range. However, because higher-order modes are supported in the large core, signal power can couple from the fundamental mode to these modes through dynamic thermo-optical scattering.¹⁹⁹ As a result, the power scaling of tapered single-frequency fiber amplifiers is often limited by TMI.

2.3. Tailoring acousto-optic interactions

In addition to the signal intensity, the SBS threshold also depends on the response of the acousto-optic medium (i.e., the fiber core) to the signal light, which is characterized by the effective Brillouin gain coefficient $g_{B,\text{eff}}$.

This coefficient scales proportionally with the material's intrinsic Brillouin gain coefficient $g_{B,0}$ and the overlap between the acoustic and optical mode profiles O , while scaling inversely with the effective Brillouin gain bandwidth $\Delta\nu_{B,\text{eff}}$. Below are three strategies that can be used to tailor the Brillouin gain in fiber amplifiers: (1) compositional engineering to reduce $g_{B,0}$,^{109–111,200} (2) structural engineering to minimize O , and (3) applying a longitudinal temperature or strain gradient to increase $\Delta\nu_{B,\text{eff}}$.

Compositional engineering. The intrinsic Brillouin gain coefficient $g_{B,0}$ at the Brillouin frequency ν_B is related to material properties by

$$g_{B,0}(\nu_B) = \frac{2\pi^2 n^7 p_{12}^2}{c\lambda_s^2 \rho V_a \Delta\nu_{B,0}}, \quad (2)$$

where n is the refractive index, p_{12} the transverse photoelastic coefficient, c the speed of light in vacuum, λ_s the signal wavelength in vacuum, ρ the density, V_a the longitudinal acoustic velocity, and $\Delta\nu_{B,0}$ the intrinsic Brillouin gain bandwidth.^{111,172,201} These quantities can be adjusted by co-doping silica (SiO_2) with Al, P, B, Ba, Sr, and/or other elements [Table 1].^{109–111,200} For instance, many dopants introduce stronger acoustic damping and thus broaden the Brillouin gain bandwidth $\Delta\nu_{B,0}$ (e.g., B_2O_3 has a particularly large $\Delta\nu_{B,0}$ of about 428 MHz, compared with 17 MHz for pure SiO_2).^{109,202,203} The p_{12} of Al_2O_3 , BaO , SrO are negative,^{203–206} which can offset the positive contributions from SiO_2 , P_2O_5 , and B_2O_3 ,^{201–203,207,208} and the p_{12} of AlPO_4 is close to zero.²⁰⁹ Careful selection of co-dopants and optimization of their concentrations are required to suppress the peak Brillouin gain while preserving the desired optical properties.^{107–110} Beyond co-doping in silica, crystal-derived glasses provide an alternative route toward exceptionally low Brillouin gain.^{210,211}

Minimizing acousto-optic overlap. The effective Brillouin gain coefficient $g_{B,\text{eff}}$ is the intrinsic Brillouin gain coefficient $g_{B,0}$ weighted by the acousto-optic overlap $|O|^2$.^{25,172,212}

$$O = \langle (\vec{\psi}_s \cdot \vec{\psi}_{St}^*) \xi^* \rangle, \quad (3)$$

where $\vec{\psi}_s$, $\vec{\psi}_{St}$, and ξ are the mode profiles of the signal, Stokes, and acoustic fields, respectively, and $\langle \cdot \rangle$ is the integral over the entire fiber cross-section. In a single-mode fiber, both the signal and Stokes fields propagate in the fundamental mode, with their profiles nearly identical due to a spectral separation of only ~ 10 GHz. There could be multiple acoustic modes in the fiber, and ξ corresponds to the one that has the greatest overlap with the optical modes.

Table 1. Effects of various dopants on the physical properties of silicate glass relevant to SBS.^{109–111} Arrows indicate increases (↑), decreases (↓), or negligible changes (≈) relative to SiO_2 upon doping.

Compound	n	ρ	V_a	$\Delta\nu_B$	p_{12}^*
SiO_2	1.45	2200 kg/m ³	5970 m/s	17 MHz	+0.226
Al_2O_3	↑	↑	↑	↑	↓
P_2O_5	↑	↑	↓	↑	↑
AlPO_4	≈	≈	↓	↑	↓
GeO_2	↑	↑	↓	↑	↑
B_2O_3	↓	↓	↓	↑	↑
BaO	↑	↑	↓	↑	↓
SrO	↑	↑	↓	↑	↓
Yb_2O_3	↑	↑	↓	↑	↓

*In the p_{12} column, downward arrows incidentally correspond to negative values, except for AlPO_4 ($p_{12} \approx 0.0$).

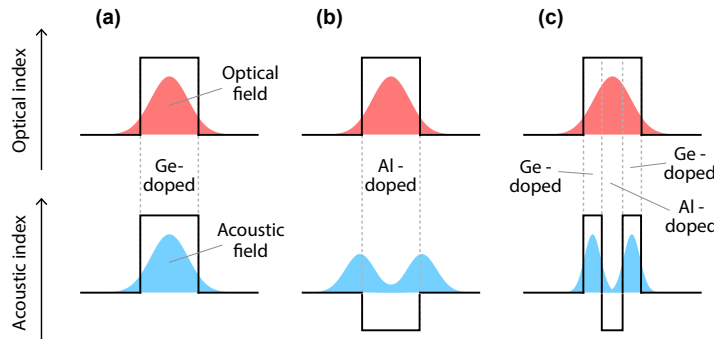


Fig. 8. **Fiber designs for reducing acousto-optic overlap.**¹⁰³ Co-dopants germanium (Ge) and aluminum (Al) both increase the optical index, but Ge raises the acoustic index, whereas Al reduces it. (a) Standard step-index fiber with a Ge-doped core, guiding both optical (upper) and acoustic (lower) fields with significant overlap. (b) Acoustically anti-guiding design using an Al-doped core. (c) Segmented doping of Al and Ge in the core, demonstrating that the acoustic and optical profiles can be independently tailored.

In step-index fibers, the uniform material composition of the core causes the optical and acoustic waves to share the same core, which maximizes the acousto-optic interaction. To suppress this interaction, a key strategy is to design microstructured fibers that decouple the acoustic and optical modes. This is made possible by the fact that co-dopants affect the optical and acoustic properties of silica glass differently [Table 1].^{102,103,109,111} For example, both Ge and Al doping increase the optical refractive in-

dex. However, while Ge doping raises the acoustic index (which is inversely proportional to V_a), Al doping lowers it. By strategically incorporating two or more co-dopants, one can design an arbitrary acoustic index profile while keeping the optical index profile unchanged [Fig. 8].^{102,103,178,186} This allows the acoustic field to be guided away from the optical intensity distribution.

In 2014, an advanced structural design incorporating three co-dopants was introduced to minimize the acousto-optic overlap in a large-core active fiber with gain confinement.¹⁶⁹ This design enabled the development of an 811-W single-frequency laser, a record that remained unbroken until 2025.^{27,169}

Temperature or strain gradient. The Brillouin frequency ν_B of a fiber depends on both temperature and strain, so applying a longitudinal gradient of temperature or strain can cause the local Brillouin frequency $\nu_B(z)$ to vary along the fiber.²¹³ This broadens the effective gain bandwidth and consequently reduces the peak gain.^{214–216} This effect is analogous to that observed in a tapered fiber, where Ω_B is similarly shifted by the change in the fiber diameter.

Heating can originate internally from the quantum defect accompanying stimulated emission, or it can be applied externally using temperature-controlled stages. As the signal is amplified along the fiber, the strongest heating occurs at which the signal power increases most rapidly.^{73,217,218} The nonuniform heating leads to longitudinal temperature gradients, observed in nearly all fiber amplifiers.^{62,73,130,217–221} Active control of the temperature gradients can be achieved by placing different fiber segments on separate temperature-controlled stages.^{45,220,222} A temperature change, $\Delta T = T' - T$, induces a linear shift in the Brillouin frequency, from $\nu_B(T)$ to $\nu_B(T')$. This relationship is given by $\nu_B(T') = \nu_B(T)[1 + C_{\text{temp}} \Delta T]$, where the scaling factor C_{temp} is typically 10^{-4} K^{-1} .²¹³ Given that $\nu_B \sim 10 \text{ GHz}$, the Brillouin frequency shifts at a rate of $\sim 1 \text{ MHz}$ per kelvin. A temperature gradient of 50–100 K can provide $\sim 100 \text{ MHz}$ of gain bandwidth broadening, effectively suppressing the SBS.^{62,204,208,214,223} When using this method, long-term operation of typical fiber amplifiers should be kept below 80°C to prevent accelerated aging of the polymer coating(s).²²¹

To apply a longitudinal strain gradient, the fiber is usually held by a series of movable fixtures.^{218,224,225} Each section of the fiber is subjected to a different tensile strain ϵ , creating a staircase-like gradient along the fiber. This strain induces a linear shift in the Brillouin frequency given by $\nu_B(\epsilon) = \nu_B(0)[1 + C_{\text{strain}}\epsilon]$, where C_{strain} is around 5 for silica fibers.²¹³

Excessive strain can damage the fiber in various ways, so the applied strain is typically limited to a few percent, which corresponds to a shift in the Brillouin frequency of up to ~ 1 GHz.²²⁵

Broadening laser linewidth. To date, single-frequency fiber amplifiers have barely reached 1 kW, with the path to access the multi-kilowatt regime requiring a significant broadening of the laser linewidth to 1–10 GHz, much wider than the Brillouin gain bandwidth.^{31–33,226} An increase in linewidth ($\Delta\nu_s$) reduces the coherence length ($L_c \sim c/\Delta\nu_s$) to ~ 1 –10 cm. While highly effective for SBS suppression and capable of retaining a useful degree of coherence for certain applications, it clearly goes beyond what is typically defined as a single-frequency laser (linewidth of MHz or below). This linewidth broadening is achieved by intentionally introducing frequency noise by phase-modulating the seed laser. Several modulation schemes are employed, including adding white noise,^{227–229} sinusoidal phase modulation,²³⁰ and pseudo-random binary sequence (PRBS).^{229,231} Among them, PRBS offers the greatest flexibility and control, allowing for optimal tailoring of the laser spectrum to maximize the SBS suppression.

3. Mitigation of Transverse Mode Instability (TMI)

3.1. *What is TMI?*

Transverse mode instability (TMI) refers to the dynamic coupling of modes caused by nonlinear thermo-optical scattering.^{26,232–237} Although single-mode fibers are designed to support only the fundamental mode, higher order modes can still exist, albeit with high loss (i.e., the power is rapidly attenuated over short distances). These modes can be excited by fiber imperfections, bending, non-ideal input coupling, or thermally induced refractive-index changes. At high power, even a very small higher-order-mode content is sufficient to trigger instability.

Consider the excitation of a single higher-order mode with power that seem negligible compared to the fundamental mode [Fig. 9(a)]. Their interference creates a shallow intensity grating. Quantum-defect heating converts the intensity grating into a temperature grating, with the brighter regions generating more heat. In silica glass, the refractive index increases with temperature, thus inducing a refractive-index grating. At low power, the heating is weak, so the induced index modulation is insufficient to cause appreciable scattering, keeping the amplifier stable. However, as the power is increased, the temperature contrast in the grating grows, which enhances

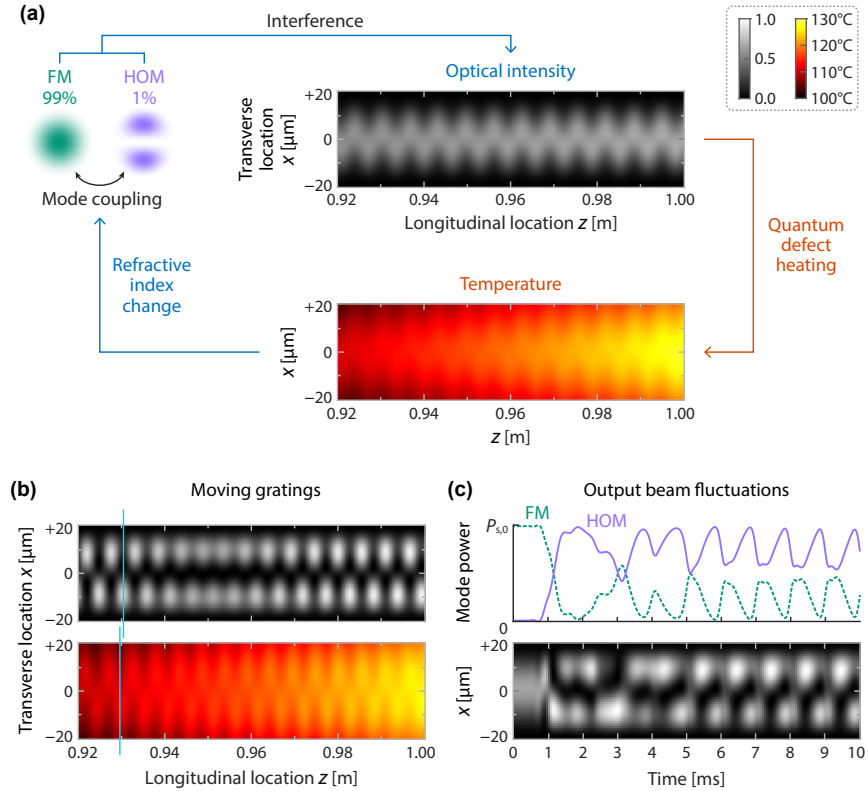


Fig. 9. **Transverse mode instability (TMI) in fiber amplifier.**²³⁸ (a) Thermo-optical feedback mechanism underlying TMI. Interference of fundamental mode (FM) and higher-order mode (HOM, 1% of input power) forms an intensity grating, which is converted into a temperature grating via quantum-defect heating. This, in turn, induces a refractive-index modulation that can transfer power between modes, altering the intensity distribution. This feedback amplifies temporal power noise in HOM and leads to TMI at high power. (b) Snapshot of TMI in fiber. Delayed thermal responses at millisecond scale create local offsets between the gratings (indicated by blue lines), causing them to “chase” each other. (c) Dynamic mode coupling (upper panel) and beam fluctuations (lower panel) at fiber output. All data are simulated using open-source codes developed by Chen *et al.*^{239,240} Ambient temperature is set at 20°C.

the index contrast. This intensified index grating scatters light more efficiently, causing power transfer between the modes, which in turn alters the intensity distribution. The redistribution of heat sources, corresponding to areas of high intensity, affects the temperature distribution. While the light responds almost instantaneously to changes in the refractive index,

the temperature distribution reacts more slowly due to heat diffusion. This delayed response causes dynamic power transfer between the modes on the millisecond scale [Fig. 9(c)]. As a result, the intensity and temperature gratings begin to “chase” each other along the fiber [Fig. 9(b)]. The output beam comprises a coherent superposition of the two modes that changes randomly and rapidly [Fig. 9(c)].

Similar to SBS, this nonlinear thermo-optical scattering acts as a noise amplifier. When no noise is present and the pump power is held constant, the beam fluctuations described above eventually diminish as the amplifier reaches a steady state. In this state, the intensity and temperature gratings are static and longitudinally aligned [Fig. 9(a)]. As can be inferred from the temperature profile, the induced index modulation is asymmetric in the transverse dimension. Within each grating period, the asymmetric index modulation in the first half scatters light from one mode to the other. In the second half, the index gradient is reversed, scattering back the same amount of light. The net power transfer is zero, and thus the overall mode content remains constant throughout the fiber. Like the input, the output power is predominantly in the fundamental mode, yielding a clean stable beam, even at high power.

However, any small temporal noise in the seed or pump power can be amplified through the thermo-optical feedback [Fig. 9(a)].²⁴¹ This noise causes signal intensity fluctuations and thus a dynamic heat load. Because the thermal response cannot follow these fluctuations instantaneously, the temperature grating lags behind, shifting it out of alignment with the intensity grating. This misalignment breaks the longitudinal symmetry of the mode-coupling process observed in the static case and yields a non-zero net power transfer. As a result, power is progressively coupled from the fundamental mode into the higher-order mode. This effectively amplifies the noise in the higher-order mode. Power then flows back and forth between the two modes, manifesting as a moving intensity grating that persists with the noise [Fig. 9(b,c)]. The resulting fluctuations in the output beam profile led to the initial discovery of TMI [Fig. 9(c)].²⁴²

The onset of TMI can be observed using a high-speed camera to monitor the entire beam^{242,243} or a photodiode to track the power fluctuations in a portion of the beam.^{244,245} The fluctuations are often quantified by their standard deviation. In many cases, a clear and abrupt increase in the standard deviation is observed with increasing pump power, and the corresponding output power is taken as the TMI threshold.^{244,245} This threshold power depends on the noise sources, their spectral characteristics

and magnitudes, and the amplifier design.

Since TMI arises from the presence of higher order modes, the most straightforward and intuitive solution is to minimize their power. This can be achieved through methods that introduce differential loss between modes, such as tight coiling,^{246,247} mode filtering,²⁴⁸ and confined doping.^{194,249,250} As these methods have already been discussed in Sec. 2.2, we will not revisit them in the following subsections.

3.2. Preventing multimode guiding at high temperature

In a typical fiber, the refractive index increases with temperature.^{108–111,251} Since the core heats up more than the cladding, their index difference grows, which makes the NA larger.²⁵² As a result, higher-order modes become less lossy, gradually turning this single-mode fiber *multimode* as power rises.

Compositional engineering. One way to address this is by designing the fiber glass so that it stays single-mode or becomes even more single-mode at high temperature.^{109,111,200} Temperature affects the refractive index of glass (n) primarily through changes in polarizability and density.^{251,253} Heating generally increases polarizability, raising the index, while thermal expansion reduces density (ρ), lowering the index. In a fiber, the core and cladding are made of different materials, so they expand at different rates when heated. If the core has a higher thermal expansion coefficient (α) than the cladding, the cladding restricts the core's expansion, creating compressive stress inside the core.¹⁰⁹ For common materials like silica, which have positive photoelastic coefficients,²⁰⁷ this compression increases the core's refractive index. The combined effect determines the thermo-optic coefficient (dn/dT). By properly mixing materials with positive dn/dT (e.g., SiO_2 , Al_2O_3 , and GeO_2) with those having negative dn/dT (e.g., P_2O_5 and B_2O_3), the refractive index can be tailored to remain nearly constant or decrease upon heating [Table 2].^{108–111,200,253}

Structural engineering. Photonic-crystal fibers offer another solution.^{254,255} The fiber structure can be designed so that, at room temperature, the signal lies outside the bandgap and thus cannot be guided. As the fiber heats up, the bandgap blue-shifts, bringing the signal into a regime where only the fundamental mode is supported. This fiber is effectively single-mode within a specific temperature range. However, two potential issues arise. First, if the fiber has not yet reached the required operating temperature, the signal power may be insufficient to suppress ASE, increasing the risk of parasitic lasing. Second, if the temperature becomes

too high, excessive bandgap shift can move the signal into a multimode regime.

Table 2. Effects of various dopants on the physical properties of silicate glass relevant to TMI.^{109–111} Arrows indicate increases (\uparrow), decreases (\downarrow), or negligible changes (\approx) relative to SiO_2 upon doping.

Compound	n	ρ	α	dn/dT^*
SiO_2	1.45	2200 kg/m^3	$0.6 \times 10^{-6} \text{ K}^{-1}$	$+1.0 \times 10^{-5} \text{ K}^{-1}$
Al_2O_3	\uparrow	\uparrow	\uparrow	\approx
P_2O_5	\uparrow	\uparrow	\uparrow	\downarrow
AlPO_4	\approx	\approx		\downarrow
GeO_2	\uparrow	\uparrow	\uparrow	\uparrow
B_2O_3	\downarrow	\downarrow	\uparrow	\downarrow
BaO	\uparrow	\uparrow	\uparrow	\uparrow
SrO	\uparrow	\uparrow	\uparrow	\downarrow
Yb_2O_3	\uparrow	\uparrow		

*In the dn/dT column, downward arrows incidentally correspond to negative values.

3.3. Gain saturation

The most common way to raise the TMI threshold is by saturating the gain with sufficient seed power to minimize local heat load.^{158,256–260} Gain saturation refers to the condition where increasing the signal power yields only a marginal increase in gain, because most excited ions are already contributing to amplification. This effectively caps the amplification, preventing excessive local energy drain and the associated heating.

The degree of gain saturation can be controlled by the pump power, which sets the level of population inversion. At low pump levels, only a small signal is needed to saturate the gain. This is why counter-pumping is generally preferred over co-pumping.^{158,256,257} By launching the pump from the end opposite the seed input, both pump and signal “increase” in power along the fiber, so the gain remains well saturated throughout. In contrast, co-pumping leaves the input end less saturated and gradually increases saturation as the signal moves down the fiber. For a double-clad fiber with a fixed signal core size, enlarging the inner cladding increases gain saturation and thereby raises the TMI threshold.^{158,256}

However, there is a practical limit to increasing gain saturation.²⁵⁶ Stronger saturation lowers the effective gain per unit length, requiring a longer fiber to reach the target output power. This comes at the cost of

a reduced SBS threshold, so properly balancing the saturation and fiber length is critical.

An effective strategy is dual-wavelength pumping.^{132,149,261} For a Yb-doped fiber amplifier, this requires pairing a strongly absorbed pump near 976 nm with a more weakly absorbed pump near 915 nm or 940 nm [Fig. 4]. By adjusting their power ratio, the degree of gain saturation can be precisely controlled. Using this approach, an all-fiber single-frequency amplifier achieving 703 W of output power was demonstrated in 2022, even under co-pumping.¹³² To mitigate the intense heating near the input inherent to co-pumping,⁷³ a longitudinally segmented doping design was employed.^{132,261–263} They spliced two fiber sections together: the first with low Yb doping to limit the peak local heat load, and the second with high Yb doping to achieve strong amplification within a short length.

The preceding sections have covered some of the mainstream strategies used in recent years to mitigate SBS and TMI. Many other innovative approaches have also been developed but are not discussed here. Examples include two-tone seeding for SBS suppression,^{217,220,264} dynamic seed or pump modulation for TMI mitigation,^{226,265,266} and single-crystalline fibers.^{267–269} Details can be found in the references cited.

4. New Strategies

Bringing single-frequency fiber lasers into the multi-kilowatt regime presents a significant technological challenge, but overcoming this barrier will push the frontiers of many laser-based technologies. To make this leap, we will likely require disruptive ideas that can fundamentally change the way we approach laser amplification. Two such promising approaches are described below.

4.1. *Multimode excitation with wavefront shaping*

Adaptive multimode fiber amplifiers have recently emerged as a promising route for further power scaling.^{175,270} This is largely because they are expected to be inherently more resistant to nonlinear optical effects than single-mode fibers.^{212,260} Analogous to chirped pulse amplification (CPA), which stretches laser pulses in time to reduce peak power, the use of multimode fibers spreads the power in space and across many spatial modes. Using a larger core reduces the intensity, which weakens light–matter interactions. Distributing the power over multiple modes further reduces non-

linear effects, as nonlinear *intermodal* scattering is generally weaker than nonlinear *intramodal* scattering within the fundamental mode. A simplified picture is the small spatial overlap between different modes, although a full analysis must also take into account mediating fields, such as acoustic modes in the case of SBS.²¹²

SBS mitigation. It has been shown, both experimentally and theoretically, that multimode excitation leads to a much higher SBS threshold than excitation of the fundamental mode alone [Fig. 10].^{171,175,212,271,272} In a multimode fiber, the signal, Stokes, and acoustic fields may each populate multiple guided modes, depending on the excitation conditions.^{212,272} As a result, SBS can occur both between modes of the same order (intramodal scattering) and between modes of different orders (intermodal scattering). The scattering from a signal mode of order l to a Stokes mode of order m is mediated primarily by one or two specific acoustic modes of j . The corresponding Brillouin gain coefficient is determined by the overlap integral of these three fields:²¹²

$$O_{mlj} = \langle (\vec{\psi}_s^{(l)} \cdot \vec{\psi}_{St}^{(m)*}) \xi^{(j)*} \rangle, \quad (4)$$

and is maximized when all are in their fundamental modes ($m = l = j = 1$), where their spatial profiles closely match. The scattering between the same higher-order optical modes ($m = l > 1$) is still primarily mediated by the fundamental acoustic mode ($j = 1$). However, the reduced spatial overlap between them leads to a lower intramodal gain than in the fundamental-mode case. For scattering between modes of different orders ($m \neq l$), the overlap is further reduced by mismatches in their spatial amplitude and polarization distributions. Also, the scattering of different signal–Stokes mode pairs (m, l) may be predominantly mediated by different acoustic modes, each characterized by its own phonon lifetime and therefore a distinct Brillouin frequency $\Omega_B^{(m,l)}$. As a result, intermodal SBS is not only weaker than intramodal gain but also spectrally separated [Fig. 10(b)].

When the signal power is distributed among multiple modes $P_{s,0} = \sum_l P_s^{(l)}(L)$ [Fig. 10(a)], the effective Brillouin gain spectrum of each Stokes mode $g_{B,eff}^{(m)}(\Omega)$ is a superposition of intramodal and intermodal gain spectra $g_B^{(m,l)}(\Omega)$, each weighted by the corresponding signal power fraction:^{212,272}

$$g_{B,eff}^{(m)}(\Omega) = \sum_l g_B^{(m,l)}(\Omega) P_s^{(l)}(L) / P_{s,0}. \quad (5)$$

In each Stokes mode, the noise-seeded power $P_{St}^{(m)}(\Omega, L)$ propagates backward from the distal end ($z = L$) and is amplified by both linear gain g_L

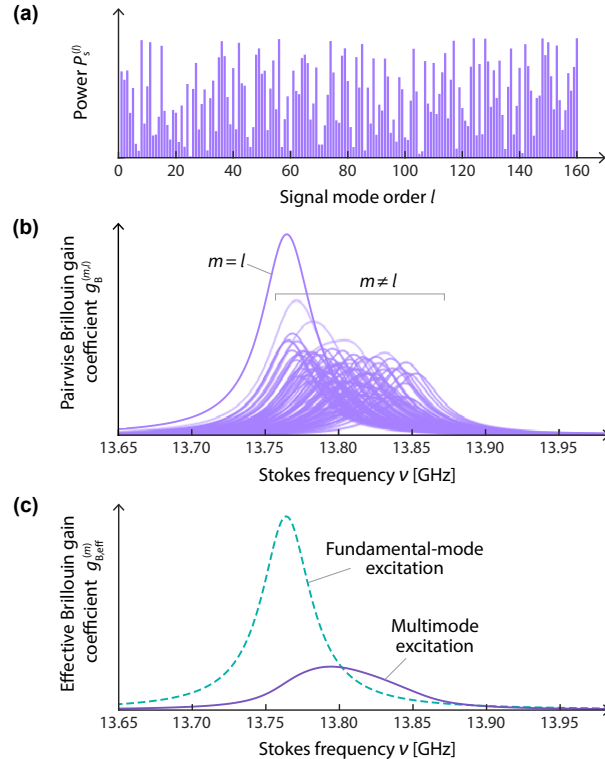


Fig. 10. Stimulated Brillouin scattering (SBS) under multimode excitation.^{175,212,271,272} (a) Signal power $P_s^{(l)}$ randomly distributed among 160 fiber modes. (b) Pairwise Brillouin gain spectra $g_B^{(m,l)}(\nu)$ experienced by a specific Stokes mode m , showing the individual contributions from various signal modes l . The intramodal gain ($m = l$) is stronger than the intermodal gain ($m \neq l$). The Stokes shift is expressed in linear frequency ν to follow experimental literature conventions. (c) Effective Brillouin gain spectrum $g_{B,eff}^{(m)}(\nu)$ for fundamental-mode excitation ($l = 1$) versus multimode excitation, where m is the mode that maximizes the effective Brillouin gain spectrum. Multimode excitation yields a broad Brillouin gain spectrum with a suppressed peak relative to the fundamental-mode-only excitation (as seen in single-mode amplifiers). All data were simulated using open-source codes developed by Wisal *et al.*¹⁷⁴

via stimulated emission and nonlinear gain $g_{B,eff}^{(m)}(\Omega)$ via SBS, leading to exponential growth toward the proximal end ($z = 0$):^{212,272}

$$P_{St}^{(m)}(\Omega, 0) = P_{St}^{(m)}(\Omega, L) e^{g_L L} e^{g_{B,eff}^{(m)}(\Omega) P_{s,0} L_{eff}}. \quad (6)$$

The Stokes mode with the largest Brillouin gain, $\max_{\Omega, m} g_{B,eff}^{(m)}(\Omega)$, dominates the growth of the total Stokes power.^{212,272}

Under multimode excitation, both the reduced scattering strengths and the spectral separation among pairwise Brillouin gain spectra contribute to a broadened effective spectrum with a low peak gain [Fig. 10(b,c)]. This stands in stark contrast to SBS in a single-mode fiber, which exhibits a strong and narrow Brillouin gain spectrum arising exclusively from fundamental-mode scattering [Fig. 10(c)]. Note also that the signal linewidth remains unaffected by multimode excitation, preserving laser coherence.^{175,271}

TMI mitigation. Counterintuitively, multimode excitation does not enhance TMI but instead mitigates it, as shown by numerical and theoretical studies^{238,260,272} with emerging experimental evidence.^{273–275}

Similar to Eq. 6 for SBS, the output noise power of mode m , $P_N^{(m)}(\Omega', L)$, can be described as the input noise power $P_N^{(m)}(\Omega', 0)$ in that mode amplified by both the linear optical gain g_L and the nonlinear thermo-optical gain $g_{T,\text{eff}}^{(m)}(\Omega')$:^{260,272}

$$P_N^{(m)}(\Omega', L) = P_N^{(m)}(\Omega', 0) e^{g_L L} e^{g_{T,\text{eff}}^{(m)}(\Omega') P_{s,0} L_{\text{eff}}}. \quad (7)$$

Here the noise is also at frequencies Stokes-shifted from the signal, $\omega_N = \omega_s - \Omega'$. This nonlinear gain coefficient $g_{T,\text{eff}}^{(m)}(\Omega')$ is given by the sum of signal powers across all contributing modes $P_s^{(l)}(\Omega', L)$ (with $l \neq m$), weighted by the intermodal thermo-optical coupling coefficient $g_T^{(m,l)}(\Omega')$, and normalized by the total signal power $P_{s,0}$:

$$g_{T,\text{eff}}^{(m)}(\Omega') = \sum_{l \neq m} g_T^{(m,l)}(\Omega') P_s^{(l)}(L) / P_{s,0}. \quad (8)$$

While common strategies for mitigating TMI involve reducing the input noise power in higher-order modes $P_N^{(m)}(\Omega', 0)$ by making them extremely lossy (see Sec. 3), the strategy discussed in this section focuses on reducing the nonlinear gain coefficient $g_{T,\text{eff}}^{(m)}(\Omega')$. Consider a fiber amplifier supporting only two modes, where the input noise power is distributed according to their signal power ratio. Equal excitation of both modes produces intensity and temperature gratings with a much higher contrast than those formed under fundamental-mode excitation (with 1% power in the higher-order mode). Although the large induced index modulation suggests stronger scattering, TMI can, in fact, be better suppressed.²³⁸

The efficacy of this approach lies in the trade-off between the input noise prefactor $P_N^{(2)}(\Omega', 0)$ and the exponential gain term $e^{g_{T,\text{eff}}^{(2)}(\Omega') P_{s,0} L_{\text{eff}}}$ [Eq. 7]. Compared to the fundamental-mode excitation, equal mode excitation increases the input noise power of the higher-order mode (by a factor

of 50). However, the nonlinear gain coefficient in the exponent is halved, because the power available for dynamic transfer (i.e., the signal power in the fundamental mode) is halved, $P_s^{(1)}(L) = P_{s,0}/2$ [Eq. 8]. For fibers of a few meters in length (large L_{eff}), this reduction significantly slows down the exponential growth of the noise power, readily outweighing the impact of the increased input noise. The TMI threshold is thereby increased, with this effect becoming even more pronounced when multiple modes are excited (as discussed shortly). Below this threshold, the output beam is stable but distorted by significant higher-order mode content. This distortion can then be corrected using one or two phase masks.²⁷⁶

It is important to note, however, that this argument (currently supported only by simulations²³⁸) contradicts recent experimental results reported by Jauregui *et al.*²³⁷ They observed a decrease in the TMI threshold when more power was allocated to the higher-order mode. This discrepancy likely arises from their use of a short fiber with a large core (and thus a long grating period), a regime which can be dominated by the input noise power rather than the nonlinear gain.

When multiple modes are excited, the optical intensity distribution in the fiber amplifier becomes speckled [Fig. 11(a)]. These intensity speckles act as localized heat sources, which generate corresponding temperature speckles. However, transverse heat diffusion smooths out the fine temperature variations, leaving only a pseudo-random thermal grating with a relatively large period [Fig. 11(b)]. As a result, the induced refractive-index grating can only efficiently couple modes with a propagation constant difference $\Delta\beta$ small enough that their beating period, $\Lambda = 2\pi/\Delta\beta$, matches the large grating period. This largely restricts the nonlinear thermo-optical scattering between neighboring modes.

In a conventional step-index fiber, each mode thermo-optically interacts with only about six effective nearest neighbors.^{238,260} If the total signal power is distributed equally among M modes ($P_s^{(l)} = P_{s,0}/M$), the nonlinear gain in Eq. 8 reduces to $g_{T,\text{eff}}^{(m)} \approx 6g_T^{(2,1)}P_{s,0}/M$, where $g_T^{(2,1)}$ is the coupling coefficient between nearest neighbors. Accordingly, the TMI threshold under multimode excitation is about $M/6$ times that under fundamental-mode excitation (as in single-mode fiber amplifiers). This indicates that the threshold increases linearly with the effective number of excited modes. For instance, exciting a few tens of modes can raise the TMI threshold by roughly an order of magnitude, from hundreds of watts to kilowatts.

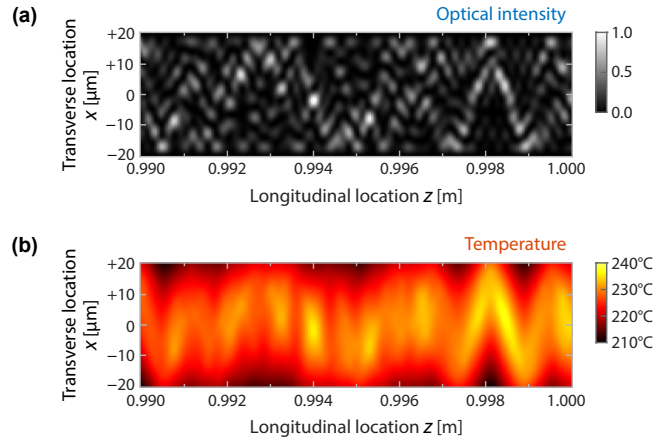


Fig. 11. Transverse mode instability (TMI) under multimode excitation.^{238,260} (a) Optical intensity and (b) temperature distributions in a fiber amplifier. Temperature speckles are much larger than intensity speckles because transverse heat diffusion smooths out fine spatial modulations. This suppresses coupling between modes with large propagation-constant difference, greatly enhancing the stability. Data are simulated using open-source codes developed by Chen *et al.*^{239,240} Ambient temperature is set at 20°C.

Wavefront shaping. Contrary to the common belief that multimode fiber amplifiers necessarily produce random speckled output, a diffraction-limited beam can be produced through coherent control of multimode amplification [Fig. 12]. The key condition is that the signal linewidth must be narrower than the spectral correlation width of the output field, which is typically on the order of gigahertz for a few meters of step-index fiber.²⁷⁷ By shaping the input seed wavefront (e.g., using a spatial light modulator), a set of modes with tailored amplitudes and phases can be selectively excited. These mode fields stay mutually coherent throughout amplification and interfere to form a desired output beam. The output beam can be diffraction-limited or, more generally, an arbitrary complex shape, provided that it can be synthesized through coherent superposition of the supported modes. The number of modes excited depends on the target beam profile and position, the fiber structure (core size, NA, and shape), and the strength of mode coupling in the fiber. Although the signal power is distributed across multiple modes within the fiber, the output field can, in principle, couple entirely into the fundamental Gaussian mode in free space and thus propagate exactly as a standard diffraction-limited beam.

Following several prior studies,^{212,238,240,260,271,276,278,279} the first experimental demonstrations of single-frequency multimode fiber amplifier were reported last year (2025), achieving output powers up to 503 W.^{175,270} By optimizing the seed wavefront to maximize the output power within a target focal area, the amplifier produces an output beam with M^2 of 1.35 that remained stable for at least several hours. Beam quality approaching the diffraction limit ($M^2 \approx 1.0$) is anticipated as the experimental apparatus and optimization algorithms are further refined.

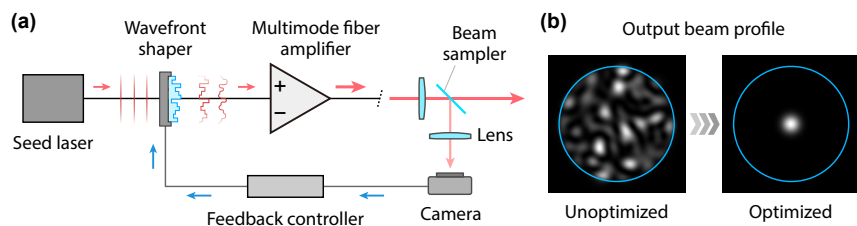


Fig. 12. **Adaptive multimode fiber amplifier.**^{175,276} (a) Input wavefront is optimized for a target output beam profile via a camera-based feedback loop. (b) Simulated output intensity profile before and after optimization of the input wavefront for a diffraction-limited output beam. Blue circles mark the core area. Mode field profiles used in the simulation were generated with open-source codes developed by Michael Hughes.²⁸⁰

4.2. Anti-Stokes fluorescence cooling

One way to suppress transverse mode instability (TMI) is to reduce the quantum defect, which is the energy difference between the pump and signal photons.^{26,79,151,152,281} The resulting heat load can be written as $Q = g_L(\lambda_s/\lambda_p - 1)I_s$, where g_L is the gain coefficient, λ_s and λ_p are the signal and pump wavelengths, and I_s is the local signal intensity. This heating decreases as the pump wavelength moves closer to the signal wavelength. While high-power diode lasers at wavelengths longer than the conventional pump wavelength (e.g., 976 nm for Yb, where absorption peaks) are technically feasible, they are rarely available commercially because there is no significant market for them. Consequently, this approach is usually implemented using tandem pumping, where one or several fiber lasers are used to pump a fiber amplifier.^{15,151–153,281}

Pushing this idea one step further, it is natural to ask whether a laser could operate without heating at all. This led to the concept of radiation-

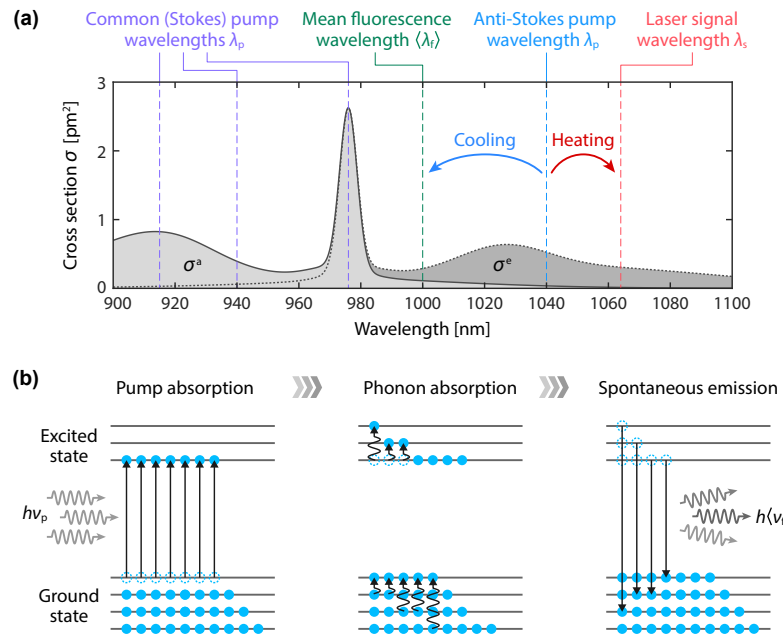


Fig. 13. **Anti-Stokes fluorescence cooling.** (a) Absorption (σ^a) and emission (σ^e) spectra of Yb^{3+} -doped silica fiber. Dashed lines are representative wavelengths for conventional and radiation-balanced laser amplification. These include common pump wavelengths λ_p at 915, 940, and 976 nm, mean fluorescence wavelength $\langle \lambda_f \rangle$ at ≈ 1000 nm, and signal wavelength λ_s at 1064 nm. Stokes pumping ($\lambda_p < \langle \lambda_f \rangle$) offers high absorption but causes heating. By contrast, anti-Stokes pumping at $\lambda_p = 1040$ nm $> \langle \lambda_f \rangle$ yields a *negative* quantum defect for spontaneous emission, which can induce cooling to counteract the heating caused by stimulated emission. Spectra were generated using open-source codes developed by Luke Rumbaugh.¹⁴¹ (b) Energy diagrams illustrating anti-Stokes fluorescence process. Low-energy pump photons excite electrons into lower sublevels of the excited state. Electrons then thermalize to higher sublevels by absorbing phonons until the Boltzmann distribution is reached. Spontaneous emission carries away more energy than supplied by the pump, leading to cooling.

balanced lasers, proposed in 1999 and demonstrated in a Yb:YAG rod in 2010 by Bowman *et al.*^{282,283} Extending this idea to fiber lasers proved much more challenging and was not achieved until 2021, when Knall *et al.* demonstrated it in a Yb-doped silicate fiber, following major advances in fiber materials and fabrication.^{284,285}

Consider a Yb-doped silicate fiber amplifier operating at a signal wavelength of $\lambda_s = 1064$ nm, with a mean fluorescence wavelength $\langle \lambda_f \rangle$ typically between 990 and 1010 nm.¹¹⁴ Although it is commonly pumped at $\lambda_p =$

915, 940, or 976 nm to ensure efficient absorption, these wavelengths are shorter than λ_s and $\langle\lambda_f\rangle$ (i.e., Stokes pumping) [Fig. 13(a)].^{15,16,157} The quantum defect is *positive* for both spontaneous and stimulated emission, and this excess photon energy is dissipated as heat.²⁸⁶

In a radiation-balanced amplifier, the pump wavelength is red-shifted beyond the mean fluorescence wavelength (anti-Stokes) but remains shorter than the signal wavelength, $\langle\lambda_f\rangle < \lambda_p < \lambda_s$, as depicted in Fig. 13(a).²⁸⁶ The anti-Stokes pump wavelength is usually selected in the range of 1030–1050 nm for optimal performance.^{287,288} These low-energy pump photons can only excite electrons from the top of the Yb^{3+} ground-state manifold to the bottom of the excited-state manifold [Fig. 13(b)]. The electrons then acquire energy from the phonon bath, allowing them to populate higher sublevels within the manifold and reach the Boltzmann distribution. Subsequent radiative relaxation to the ground state via spontaneous emission carries this energy out of the fiber. Since the average energy of the emitted photons ($h\langle\nu_f\rangle$) exceeds that of the absorbed pump photons ($h\nu_p$), the fiber is cooled. This process is commonly referred to as anti-Stokes fluorescence cooling. The maximum heat extraction rate per unit length is given by:

$$\left(\frac{dQ}{dt}\right)_{\max} = \left(\frac{\tau_{\text{rad}}}{\tau(N_0)}h\nu_p - h\langle\nu_f\rangle\right) \frac{\sigma_p^a}{\sigma_p^a + \sigma_p^e} \frac{A_0 N_0}{\tau_{\text{rad}}}, \quad (9)$$

where N_0 is the Yb^{3+} concentration, A_0 is the doped area, τ_{rad} is the radiative lifetime, $\tau(N_0)$ is the concentration-dependent excited-state lifetime (as shortened by quenching), σ_p^a and σ_p^e are the absorption and emission cross-sections at the pump wavelength. When this cooling balances the heat generated during signal amplification, the amplifier can operate at room temperature with zero net heating.

Net cooling by anti-Stokes pumping does not occur in all fiber amplifiers. In most commercial fibers, parasitic heating from impurity absorption, concentration quenching, and photodarkening can readily outpace heat extraction by anti-Stokes fluorescence, causing the fiber to heat up even at low pump powers.^{289–291} With advances in materials engineering,^{114,292} radiation-balanced amplification of single-frequency lasers has been demonstrated at output powers of up to 600 mW.^{284,285,293–295} Even when scaling to the 1–10 W level, the temperature rise of these fiber amplifiers remains within a few kelvins when suspended in air, as parasitic effects are effectively suppressed.²⁹⁶

Scaling to hundred-watt output comparable to state-of-the-art amplifiers is a non-trivial task. One major challenge is the need for much stronger

cooling. Another is ensuring sufficient gain, which likely requires a longer fiber (potentially tens of meters) because the absorption cross-section σ_p^a at anti-Stokes pump wavelengths is much lower than that at conventional (Stokes) pump wavelengths.²⁸⁶ However, increasing the fiber length lowers the SBS threshold.

Equation 9 suggests two pathways for enhancing cooling. The first is to further increase the rare-earth doping concentration N_0 beyond the typical range of 10^{25} – 10^{27} Yb/m³, which increases both cooling and gain per unit length. This, however, often comes with stronger quenching and higher density of impurities. Effective suppression of parasitic effects at very high doping levels is essential and requires optimization of both glass composition and fiber fabrication.^{79,114} The second is to increase the doped area A_0 , which enhances not only the achievable cooling but also the pump saturation power, allowing higher pump injection. This inevitably results in multimode operation. As discussed in Sec. 4.1, high beam quality can be maintained through seed-wavefront shaping, and the SBS threshold is effectively increased due to reduced intensity and multimode excitation.¹⁷⁵

Along similar lines, excitation-balanced amplification has been proposed to achieve athermal operation.^{297,298} The active fiber is pumped at two wavelengths: one shorter (Stokes) and one longer (anti-Stokes) than the signal wavelength. The quantum-defect heating from the former is balanced by the cooling from the latter. While this concept has been validated numerically and supported by preliminary experimental checks, it still awaits further experimental demonstration to confirm its practical efficacy.

5. Beyond Current Limits

While the mitigation of nonlinear acousto- and thermo-optical scattering remains the primary focus for high-power single-frequency fiber amplifiers, continued power scaling will inevitably bring other nonlinear physical processes into play. Most of these nonlinear optical effects are essentially a result of optical noise amplification driven by nonlinear physical processes.^{62,212,233,241,260} Even if the nonlinear effects are not severe enough to prevent increased output power from the amplifier, their presence can still lead to noisy output, which significantly degrades system performance.^{47,175,299} Therefore, bold ideas for mitigating nonlinear effects are always welcomed.

The goal of designing high-power single-frequency fiber amplifiers shares a similar spirit with the peace sought in this classic bedtime ritual, where every unwanted disturbance must be hushed:

*Goodnight stars,
Goodnight air,
Goodnight noises everywhere.*

— *Goodnight Moon* by Margaret Wise Brown

6. Acknowledgments

I would like to thank Prof. Hui Cao at Yale University, Dr. Peyman Ahmadi at Tescan, and Dr. Kabish Wisal at ASML for their feedback during the writing of this chapter and Dr. Ting-Mao Feng at National Sun Yat-sen University for his assistance in preparing the figures.

Beyond these specific contributions, I am sincerely appreciative of the support and guidance provided by Prof. Hui Cao, Prof. Michel J. F. Digonnet at Stanford University, Prof. Iam Choon Khoo at Penn State University, and Prof. Tsung-Hsien Lin at National Sun Yat-sen University over the years. I am also grateful to all the brilliant minds I've had the privilege to work with and learn from.

This book chapter is dedicated to my partner Shuo, my sisters Yu-yu and Ning-ning, and my children Bailey, Mochi, Rary (Laurie), and Robin.

References

1. K. Kikuchi, Fundamentals of coherent optical fiber communications, *Journal of lightwave technology*. **34**(1), 157–179 (2015).
2. Y. Kawahito, H. Wang, S. Katayama, and D. Sumimori, Ultra high power (100 kW) fiber laser welding of steel, *Optics Letters*. **43**(19), 4667–4670 (2018).
3. A. R. Bakhtari, H. K. Sezer, O. E. Canyurt, O. Eren, M. Shah, and S. Marimuthu, A Review on Laser Beam Shaping Application in Laser-Powder Bed Fusion, *Advanced Engineering Materials*. **26**(14), 2302013 (2024).
4. J.-P. Cariou, B. Augere, and M. Valla, Laser source requirements for coherent lidars based on fiber technology, *Comptes Rendus Physique*. **7**(2), 213–223 (2006).
5. G. Canat, B. Augère, C. Besson, A. Dolfi-Bouteyre, A. Durecu, D. Gouilar,

J. Le Gouët, L. Lombard, C. Planchat, and M. Valla. High peak power single-frequency MOPFA for lidar applications. In *CLEO: Applications and Technology*, pp. AM3K–4 (2016).

- 6. K. Wang, C. Gao, Z. Lin, Q. Wang, M. Gao, S. Huang, and C. Chen, 1645 nm coherent Doppler wind lidar with a single-frequency Er: YAG laser, *Optics Express*. **28**(10), 14694–14704 (2020).
- 7. J. Grandidier, P. Jaffe, W. T. Roberts, M. W. Wright, A. A. Fraeman, C. A. Raymond, A. Austin, P. Lubin, E. T. Sunada, J.-P. Jones, et al., Laser power beaming for lunar night and permanently shadowed regions, *Jet Propulsion*. **818**, 354–1566 (2021).
- 8. T. Karr and J. Trebes, The new laser weapons, *Physics Today*. **77**(1), 32–38 (2024).
- 9. R. Holten, A. Flores, T. Ehrenreich, B. Anderson, and I. Dajani. Beam-combinable high-power fiber laser sources for directed energy applications. In *High-Power Laser Ablation VIII*, vol. 12939, pp. 81–88 (2024).
- 10. E. Rochat, R. Dandliker, K. Haroud, R. H. Czichy, U. Roth, D. Costantini, and R. Holzner, Fiber amplifiers for coherent space communication, *IEEE Journal of Selected Topics in Quantum Electronics*. **7**(1), 64–80 (2001).
- 11. W. Y. Anthony. Fiber lasers and amplifiers for space Lidar applications. In *Sixth International Workshop on Specialty Optical Fibers and Their Applications (WSOF 2019)*, vol. 11206, pp. 1120606–1 (2019).
- 12. T. J. Karr, Synthetic aperture Ladar for high-resolution ground-based imaging of objects in LEO, GEO, and Cis-Lunar space, *IEEE Transactions on Aerospace and Electronic Systems*. **60**(4), 5499–5514 (2024).
- 13. M. J. Digonnet, *Rare-earth-doped fiber lasers and amplifiers, revised and expanded*. CRC press (2001).
- 14. L. Zenteno, High-power double-clad fiber lasers, *Journal of Lightwave Technology*. **11**(9), 1435–1446 (2002).
- 15. D. J. Richardson, J. Nilsson, and W. A. Clarkson, High power fiber lasers: current status and future perspectives, *Journal of the Optical Society of America B*. **27**(11), B63–B92 (2010).
- 16. C. Jauregui, J. Limpert, and A. Tünnermann, High-power fibre lasers, *Nature Photonics*. **7**(11), 861–867 (2013).
- 17. M. N. Zervas and C. A. Codemard, High power fiber lasers: a review, *IEEE Journal of selected topics in Quantum Electronics*. **20**(5), 219–241 (2014).
- 18. L. Dong and M. N. Zervas, Past, present, and future of fiber lasers and amplifiers, *Optics Communications*. **577**, 131419 (2025).
- 19. S. Fu, W. Shi, Y. Feng, L. Zhang, Z. Yang, S. Xu, X. Zhu, R. A. Norwood, and N. Peyghambarian, Review of recent progress on single-frequency fiber lasers, *Journal of the Optical Society of America B*. **34**(3), A49–A57 (2017).
- 20. C. Li, Y. Tao, M. Jiang, P. Ma, W. Liu, R. Su, J. Xu, J. Leng, and P. Zhou, High-power single-frequency fiber amplifiers: progress and challenge, *Chinese Optics Letters*. **21**(9), 090002 (2023).
- 21. G. Di Domenico, S. Schilt, and P. Thomann, Simple approach to the relation between laser frequency noise and laser line shape, *Applied Optics*. **49**(25), 4801–4807 (2010).

22. K.-H. Lee, K. Lee, Y. Kim, Y.-H. Cha, G. Lim, H. Park, H. Cho, and D.-Y. Jeong, Transverse mode instability induced by stimulated Brillouin scattering in a pulsed single-frequency large-core fiber amplifier, *Applied Optics*. **54**(2), 189–194 (2015).
23. Y. Panbhiharwala, A. V. Harish, D. Venkitesh, J. Nilsson, and B. Srinivasan, Investigation of temporal dynamics due to stimulated Brillouin scattering using statistical correlation in a narrow-linewidth cw high power fiber amplifier, *Optics Express*. **26**(25), 33409–33417 (2018).
24. J. Young, A. Goers, D. Brown, M. Dennis, K. Lehr, C. Wei, C. Menyuk, and J. Hu, Tradeoff between the Brillouin and transverse mode instabilities in Yb-doped fiber amplifiers, *Optics Express*. **30**(22), 40691–40703 (2022).
25. A. Kobyakov, M. Sauer, and D. Chowdhury, Stimulated Brillouin scattering in optical fibers, *Advances in optics and photonics*. **2**(1), 1–59 (2009).
26. C. Jauregui, C. Stihler, and J. Limpert, Transverse mode instability, *Advances in Optics and Photonics*. **12**(2), 429–484 (2020).
27. W. Li, W. Liu, Y. Deng, Y. Chen, H. Yang, Q. Chen, J. Zheng, H. Xiao, Z. Chen, Z. Pan, P. Ma, Z. Wang, L. Si, S. Xu, and J. Chen, Functional Yb-doped fiber with a bat-type refractive index distribution for beyond kilowatt all-fiber single-frequency laser amplification, *Light: Science & Applications*. **14**(1), 271 (2025).
28. H. Fathi, M. Närhi, and R. Gumeyuk. Towards ultimate high-power scaling: Coherent beam combining of fiber lasers. In *Photonics*, vol. 8, p. 566 (2021).
29. C. L. Linslal, P. Ayyaswamy, S. Maji, M. S. Sooraj, A. Dixit, D. Venkitesh, and B. Srinivasan, Challenges in coherent beam combining of high power fiber amplifiers: a review, *ISSS Journal of Micro and Smart Systems*. **11**(1), 277–293 (2022).
30. C. Akcay, P. Parrein, and J. P. Rolland, Estimation of longitudinal resolution in optical coherence imaging, *Applied optics*. **41**(25), 5256–5262 (2002).
31. D. Creeden, M. Underwood, T. G. D’Alberto, T. Tero, D. Hosmer, R. Basque, J. Galipeau, J. Sears, D. Paquette, and C. Ebert. Advanced packaging and power scaling of narrow linewidth fiber amplifiers. In *Laser Technology for Defense and Security XIV*, vol. 10637, pp. 8–14 (2018).
32. J. W. Nicholson, J. Pincha, I. Kansal, R. S. Windeler, E. Monberg, V. Lukonin, A. Hariharan, G. Williams, A. Rosales-Garcia, L. Bansal, et al. 5 kW single-mode output power from Yb-doped fibers with increased higher-order mode loss. In *Fiber Lasers XX: Technology and Systems*, vol. 12400, p. 1240002 (2023).
33. J. Edgecumbe and D. Martz. Fiber lasers for directed energy. In *High-Power Laser Ablation VIII*, vol. 12939, pp. 75–80 (2024).
34. M. M. Bayer, X. Li, G. N. Guentchev, R. Torun, J. E. Velazco, and O. Boyraz, Single-shot ranging and velocimetry with a CW lidar far beyond the coherence length of the CW laser, *Optics Express*. **29**(26), 42343–42354 (2021).
35. A. Atalar, C. J. Margison, M. M. Bayer, X. Li, O. B. Boyraz, and O. Boyraz, 3D coherent single shot lidar imaging beyond coherence length, *Optics Ex-*

press. **32**(23), 40783–40793 (2024).

- 36. R. D. Richmond and S. C. Cain, *Direct-Detection LADAR Systems*. SPIE Press. Tutorial Texts in Optical Engineering, volume TT85, Bellingham, Washington, USA (2010). ISBN 978-0-8194-8072-9.
- 37. T. T. Lyons, M. W. Regehr, and F. J. Raab, Shot noise in gravitational-wave detectors with Fabry–Perot arms, *Applied Optics*. **39**(36), 6761–6770 (2000).
- 38. B. Willke, K. Danzmann, M. Frede, P. King, D. Kracht, P. Kwee, O. Puncken, R. Savage, B. Schulz, F. Seifert, et al., Stabilized lasers for advanced gravitational wave detectors, *Classical and Quantum Gravity*. **25**(11), 114040 (2008).
- 39. B. Willke, Stabilized lasers for advanced gravitational wave detectors, *Laser & Photonics Reviews*. **4**(6), 780–794 (2010).
- 40. P. Kwee, C. Bogan, K. Danzmann, M. Frede, H. Kim, P. King, J. Pöld, O. Puncken, R. L. Savage, F. Seifert, et al., Stabilized high-power laser system for the gravitational wave detector advanced LIGO, *Optics Express*. **20**(10), 10617–10634 (2012).
- 41. E. Hall. Laser Frequency and Intensity Stabilization for Advanced LIGO. In *18th Coherent Laser Radar Conference and the Lidar Working Group on Space Based Winds, CLRC 2016* (2016).
- 42. M. Steinke, H. Tuennermann, V. Kuhn, T. Theeg, M. Karow, O. de Varona, P. Jahn, P. Booker, J. Neumann, P. Wessels, et al., Single-frequency fiber amplifiers for next-generation gravitational wave detectors, *IEEE Journal of Selected Topics in Quantum Electronics*. **24**(3), 1–13 (2017).
- 43. O. De Varona, W. Fittkau, P. Booker, T. Theeg, M. Steinke, D. Kracht, J. Neumann, and P. Wessels, Single-frequency fiber amplifier at 1.5 μ m with 100 W in the linearly-polarized TEM₀₀ mode for next-generation gravitational wave detectors, *Optics Express*. **25**(21), 24880–24892 (2017).
- 44. A. Buikema, F. Jose, S. J. Augst, P. Fritschel, and N. Mavalvala, Narrow-linewidth fiber amplifier for gravitational-wave detectors, *Optics Letters*. **44**(15), 3833–3836 (2019).
- 45. F. Wellmann, M. Steinke, F. Meylahn, N. Bode, B. Willke, L. Overmeyer, J. Neumann, and D. Kracht, High power, single-frequency, monolithic fiber amplifier for the next generation of gravitational wave detectors, *Optics Express*. **27**(20), 28523–28533 (2019).
- 46. D. Kapasi, J. Eichholz, T. McRae, R. Ward, B. Slagmolen, S. Legge, K. Hardman, P. Altin, and D. McClelland, Tunable narrow-linewidth laser at 2 μ m wavelength for gravitational wave detector research, *Optics Express*. **28**(3), 3280–3288 (2020).
- 47. S. Hochheim, E. Brockmüller, P. Wessels, J. Koponen, T. Lowder, S. Novotny, B. Willke, J. Neumann, and D. Kracht, Single-frequency 336 W spliceless all-fiber amplifier based on a chirally-coupled-core fiber for the next generation of gravitational wave detectors, *Journal of Lightwave Technology*. **40**(7), 2136–2143 (2021).
- 48. F. Wellmann, N. Bode, P. Wessels, L. Overmeyer, J. Neumann, B. Willke, and D. Kracht, Low noise 400 W coherently combined single frequency laser

beam for next generation gravitational wave detectors, *Optics Express*. **29** (7), 10140–10149 (2021).

- 49. C. Cahillane, G. L. Mansell, and D. Sigg, Laser frequency noise in next generation gravitational-wave detectors, *Optics Express*. **29**(25), 42144–42161 (2021).
- 50. F. Meylahn, N. Knust, and B. Willke, Stabilized laser system at 1550 nm wavelength for future gravitational-wave detectors, *Physical Review D*. **105** (12), 122004 (2022).
- 51. W. Jia, H. Yamamoto, K. Kuns, A. Effler, M. Evans, P. Fritschel, R. Abbott, C. Adams, R. X. Adhikari, A. Ananyeva, et al., Point absorber limits to future gravitational-wave detectors, *Physical Review Letters*. **127**(24), 241102 (2021).
- 52. C. J. Koester and E. Snitzer, Amplification in a fiber laser, *Applied Optics*. **3**(10), 1182–1186 (1964).
- 53. S. Sinha, K. E. Urbanek, A. Krzywicki, and R. L. Byer, Investigation of the suitability of silicate bonding for facet termination in active fiber devices, *Optics Express*. **15**(20), 13003–13022 (2007).
- 54. Y. O. Aydin, F. Maes, V. Fortin, S. T. Bah, R. Vallée, and M. Bernier, Endcapping of high-power 3 μ m fiber lasers, *Optics Express*. **27**(15), 20659–20669 (2019).
- 55. J. Nicholson, A. DeSantolo, P. Westbrook, R. Windeler, T. Kremp, C. Headley, and D. DiGiovanni, Axicons for mode conversion in high peak power, higher-order mode, fiber amplifiers, *Optics Express*. **23**(26), 33849–33860 (2015).
- 56. L. Han, M. Hao, L. Tao, and J. Li, Fiber combiner terminated with quartz block head for direct beam combining of fiber coupled laser diodes, *Optik*. **184**, 35–39 (2019).
- 57. X. Chen, T. Yao, L. Huang, Y. An, H. Wu, Z. Pan, and P. Zhou, Functional fibers and functional fiber-based components for high-power lasers, *Advanced Fiber Materials*. **5**(1), 59–106 (2023).
- 58. K. Boyd, N. Simakov, A. Hemming, J. Daniel, R. Swain, E. Mies, S. Rees, W. Andrew Clarkson, and J. Haub, CO₂ laser-fabricated cladding light strippers for high-power fiber lasers and amplifiers, *Applied Optics*. **55**(11), 2915–2920 (2016).
- 59. P. Yan, J. Sun, Y. Huang, D. Li, X. Wang, Q. Xiao, and M. Gong, Kilowatt-level cladding light stripper for high-power fiber laser, *Applied Optics*. **56** (7), 1935–1939 (2017).
- 60. Y. Liu, S. Huang, W. Wu, P. Zhao, X. Tang, X. Feng, M. Li, B. Shen, H. Song, R. Tao, et al., 2 kW high stability robust fiber cladding mode stripper with moderate package temperature rising, *IEEE Photonics Technology Letters*. **32**(18), 1151–1154 (2020).
- 61. M. Mermelstein, K. Brar, M. Andrejco, A. Yablon, M. Fishteyn, C. Headley, and D. DiGiovanni. All-fiber 194 W single-frequency single-mode Yb-doped master-oscillator power-amplifier. In *LEOS 2007-IEEE Lasers and Electro-Optics Society Annual Meeting Conference Proceedings*, pp. 382–383 (2007).
- 62. M. Hildebrandt, S. Büsche, P. Weßels, M. Frede, and D. Kracht, Brillouin

scattering spectra in high-power single-frequency ytterbium doped fiber amplifiers, *Optics Express*. **16**(20), 15970–15979 (2008).

- 63. C. Zeng, W. Peng, Q. Zhao, W. Lin, C. Yang, Y. Sun, C. Wang, Z. Feng, Z. Yang, and S. Xu, Simultaneous achievement of power boost and low-frequency intensity noise suppression in a bidirectional pumping fiber amplifier based on saturated even-distribution gain, *Optics Express*. **31**(3), 5122–5130 (2023).
- 64. B. Morasse, A. Perron, D. Faucher, P.-M. Belzile, M. V. Deschênes, F. Faucher, G. Brochu, F. Trépanier, and P. Deladurantaye, Efficient 1018nm high power fiber laser using intracavity tilted FBG ASE filters. In *Fiber Lasers XXI: Technology and Systems*, vol. 12865, pp. 40–49 (2024).
- 65. A. Leleux, Y. O. Aydin, W. Bisson, A. Michaud, A. Karim, A. Mehaboob, I. Carvalho Pinto, N. Boessinger, M. Esplingand, J. Moriamez, et al., High power neodymium-doped single-mode all-fiber laser at 922 nm using chirped tilted fiber Bragg gratings, *Optics Express*. **33**(22), 46485–46493 (2025).
- 66. M. Davis, M. Digonnet, R. H. Pantell, and L. Fellow, Thermal effects in doped fibers, *Journal of Lightwave Technology*. **16**(6), 1013 (1998).
- 67. D. C. Brown and H. J. Hoffman, Thermal, stress, and thermo-optic effects in high average power double-clad silica fiber lasers, *IEEE Journal of Quantum Electronics*. **37**(2), 207–217 (2001).
- 68. Y. Wang, C.-Q. Xu, and H. Po, Thermal effects in kilowatt fiber lasers, *IEEE Photonics Technology Letters*. **16**(1), 63–65 (2004).
- 69. A. Galvanauskas, High power fiber lasers, *Optics and photonics news*. **15**(7), 42–47 (2004).
- 70. L. Li, H. Li, T. Qiu, V. Temyanko, M. Morrell, A. Schülzgen, A. Mafi, J. Moloney, and N. Peyghambarian, 3-Dimensional thermal analysis and active cooling of short-length high-power fiber lasers, *Optics Express*. **13**(9), 3420–3428 (2005).
- 71. M.-A. Lapointe, S. Chatigny, M. Piché, M. Cain-Skaff, and J.-N. Maran, Thermal effects in high-power CW fiber lasers. In *Fiber lasers VI: technology, systems, and applications*, vol. 7195, pp. 430–440 (2009).
- 72. A. A. Stolov, D. A. Simoff, and J. Li, Thermal stability of specialty optical fibers, *Journal of Lightwave Technology*. **26**(20), 3443–3451 (2009).
- 73. K. R. Hansen, T. T. Alkeskjold, J. Broeng, and J. Lægsgaard, Thermo-optical effects in high-power ytterbium-doped fiber amplifiers, *Optics Express*. **19**(24), 23965–23980 (2011).
- 74. Y. Fan, B. He, J. Zhou, J. Zheng, H. Liu, Y. Wei, J. Dong, and Q. Lou, Thermal effects in kilowatt all-fiber MOPA, *Optics Express*. **19**(16), 15162–15172 (2011).
- 75. L. Dong, Thermal lensing in optical fibers, *Optics Express*. **24**(17), 19841–19852 (2016).
- 76. J. M. Daniel, N. Simakov, A. Hemming, W. A. Clarkson, and J. Haub, Metal clad active fibres for power scaling and thermal management at kW power levels, *Optics Express*. **24**(16), 18592–18606 (2016).
- 77. X. Y. Charles, O. Shatrovoy, T. Fan, and T. Taunay, Diode-pumped narrow linewidth multi-kW metalized Yb fiber amplifier. In *Advanced Solid State*

Lasers, pp. ATu6A–1 (2016).

- 78. M. N. Zervas, Transverse mode instability, thermal lensing and power scaling in Yb^{3+} -doped high-power fiber amplifiers, *Optics Express*. **27**(13), 19019–19041 (2019).
- 79. J. Ballato, P. D. Dragic, and M. J. Digonnet, Prospects and challenges for all-optical thermal management of fiber lasers, *Journal of Physics D: Applied Physics*. **57**(16), 162001 (2024).
- 80. E. Snitzer, H. Po, F. Hakimi, R. Tumminelli, and B. McCollum. Double clad, offset core Nd fiber laser. In *Optical fiber sensors*, p. PD5 (1988).
- 81. H. Po, E. Snitzer, R. Tumminelli, L. Zenteno, F. Hakimi, N. M. Cho, and T. Haw. Double clad high brightness Nd fiber laser pumped by GaAlAs phased array. In *Optical Fiber Communication Conference*, p. PD7 (1989).
- 82. P. Leproux, S. Février, V. Doya, P. Roy, and D. Pagnoux, Modeling and optimization of double-clad fiber amplifiers using chaotic propagation of the pump, *Optical Fiber Technology*. **7**(4), 324–339 (2001).
- 83. D. Kouznetsov, J. V. Moloney, and E. M. Wright, Efficiency of pump absorption in double-clad fiber amplifiers. I. Fiber with circular symmetry, *Journal of the Optical Society of America B*. **18**(6), 743–749 (2001).
- 84. N. A. Mortensen, Air-clad fibers: pump absorption assisted by chaotic wave dynamics?, *Optics Express*. **15**(14), 8988–8996 (2007).
- 85. P. Koška, P. Peterka, J. Aubrecht, O. Podrazký, F. Todorov, M. Becker, Y. Baravets, P. Honzátko, and I. Kašík, Enhanced pump absorption efficiency in coiled and twisted double-clad thulium-doped fibers, *Optics Express*. **24**(1), 102–107 (2016).
- 86. Y. Li, S. D. Jackson, and S. Fleming, High absorption and low splice loss properties of hexagonal double-clad fiber, *IEEE Photonics Technology Letters*. **16**(11), 2502–2504 (2004).
- 87. A. Tünnermann, T. Schreiber, and J. Limpert, Fiber lasers and amplifiers: an ultrafast performance evolution, *Applied Optics*. **49**(25), F71–F78 (2010).
- 88. D. Kouznetsov and J. V. Moloney, Efficiency of pump absorption in double-clad fiber amplifiers. II. Broken circular symmetry, *Journal of the Optical Society of America B*. **19**(6), 1259–1263 (2002).
- 89. V. Doya, O. Legrand, and F. Mortessagne, Optimized absorption in a chaotic double-clad fiber amplifier, *Optics Letters*. **26**(12), 872–874 (2001).
- 90. D. Kouznetsov and J. V. Moloney, Efficiency of pump absorption in double-clad fiber amplifiers. III. Calculation of modes, *Journal of the Optical Society of America B*. **19**(6), 1304–1309 (2002).
- 91. S. D. Jackson, Towards high-power mid-infrared emission from a fibre laser, *Nature Photonics*. **6**(7), 423–431 (2012).
- 92. S. Tanabe, Rare-earth-doped glasses for fiber amplifiers in broadband telecommunication, *Comptes Rendus Chimie*. **5**(12), 815–824 (2002).
- 93. X. Zhu and N. Peyghambarian, High-power ZBLAN glass fiber lasers: Review and prospect, *Advances in OptoElectronics*. **2010**(1), 501956 (2010).
- 94. M. Bernier, Y. O. Aydin, P. Paradis, V. Fortin, W. Bisson, A. Michaud, L.-C. Michaud, T. Boilard, M. Lemieux-Tanguay, L. Talbot, et al. Get the most out of a fiber laser: from high-power CW to ultrafast operation, from visible

to mid-infrared emission. In *Fiber Lasers XXII: Technology and Systems*, vol. 13342, pp. 10–12 (2025).

95. R. Paschotta, J. Nilsson, A. C. Tropper, and D. C. Hanna, Ytterbium-doped fiber amplifiers, *IEEE Journal of Quantum Electronics*. **33**(7), 1049–1056 (2002).
96. P. M. Becker, A. A. Olsson, and J. R. Simpson, *Erbium-doped fiber amplifiers: fundamentals and technology*. Elsevier (1999).
97. A. Sincore, J. D. Bradford, J. Cook, L. Shah, and M. C. Richardson, High average power thulium-doped silica fiber lasers: review of systems and concepts, *IEEE Journal of selected topics in quantum electronics*. **24**(3), 1–8 (2017).
98. C. Gaida, M. Gebhardt, T. Heuermann, F. Stutzki, C. Jauregui, and J. Limpert, Ultrafast thulium fiber laser system emitting more than 1 kW of average power, *Optics Letters*. **43**(23), 5853–5856 (2018).
99. M. Fermann, D. Hanna, D. Shepherd, P. Suni, and J. Townsend, Efficient operation of an Yb-sensitised Er fibre laser at 1.56 μ m, *Electronics Letters*. **24**(18), 1135–1136 (1988).
100. M. Pollnau and S. D. Jackson, Advances in mid-infrared fiber lasers. In *Mid-infrared coherent sources and applications*, pp. 315–346. Springer (2008).
101. J. Nilsson, S.-U. Alam, J. A. Alvarez-Chavez, P. W. Turner, W. A. Clarkson, and A. B. Grudinin, High-power and tunable operation of erbium-ytterbium co-doped cladding-pumped fiber lasers, *IEEE Journal of Quantum Electronics*. **39**(8), 987–994 (2003).
102. S. Gray, D. Walton, J. Wang, M.-J. Li, X. Chen, A. B. Ruffin, J. Demeritt, and L. Zenteno, High power, narrow linewidth fiber amplifiers. In *Optical Amplifiers and their Applications*, p. OSuB1 (2006).
103. M.-J. Li, X. Chen, J. Wang, S. Gray, A. Liu, J. A. Demeritt, A. B. Ruffin, A. M. Crowley, D. T. Walton, and L. A. Zenteno, Al/Ge co-doped large mode area fiber with high SBS threshold, *Optics Express*. **15**(13), 8290–8299 (2007).
104. J. Lucas, Infrared glasses, *Current Opinion in Solid State and Materials Science*. **4**(2), 181–187 (1999).
105. P. D. Dragic, M. Cavillon, and J. Ballato, Materials for optical fiber lasers: A review, *Applied Physics Reviews*. **5**(4) (2018).
106. M. Engholm, P. Jelger, F. Laurell, and L. Norin, Improved photodarkening resistivity in ytterbium-doped fiber lasers by cerium codoping, *Optics Letters*. **34**(8), 1285–1287 (2009).
107. J. Ballato, M. Cavillon, and P. Dragic, A unified materials approach to mitigating optical nonlinearities in optical fiber. I. Thermodynamics of optical scattering, *International Journal of Applied Glass Science*. **9**(2), 263–277 (2018).
108. P. D. Dragic, M. Cavillon, A. Ballato, and J. Ballato, A unified materials approach to mitigating optical nonlinearities in optical fiber. II. A. Material additivity models and basic glass properties, *International Journal of Applied Glass Science*. **9**(2), 278–287 (2018).
109. P. D. Dragic, M. Cavillon, A. Ballato, and J. Ballato, A unified materials

approach to mitigating optical nonlinearities in optical fiber. II. B. The optical fiber, material additivity and the nonlinear coefficients, *International Journal of Applied Glass Science*. **9**(3), 307–318 (2018).

110. M. Cavillon, C. Kucera, T. Hawkins, J. Dawson, P. D. Dragic, and J. Ballato, A unified materials approach to mitigating optical nonlinearities in optical fiber. III. Canonical examples and materials road map, *International Journal of Applied Glass Science*. **9**(4), 447–470 (2018).
111. T. Hawkins, P. Dragic, N. Yu, A. Flores, and J. Ballato, Kilowatt power scaling of an intrinsically low Brillouin and thermo-optic Yb-doped silica fiber, *Journal of the Optical Society of America B*. **38**(12), F38–F49 (2021).
112. G. Xiang, H. Zhang, X. Wang, J. Zhang, H. Chen, C. Lin, Y. Ye, W. Hua, and J. Chen, Fully recoverable fiber lasers under radiation enabled by in-situ blue light photobleaching, *Photonics Research*. **13**(8), 2362–2370 (2025).
113. J. Ballato and P. Dragic, Rethinking optical fiber: new demands, old glasses, *Journal of the American Ceramic Society*. **96**(9), 2675–2692 (2013).
114. C.-W. Chen, B. Meehan, M. A. Cahoon, T. W. Hawkins, J. Ballato, P. D. Dragic, M. Engholm, T. Boilard, M. Bernier, and M. J. Digonnet, Emerging trends in laser-cooling of Yb-doped silicate fibers, *Journal of Lightwave Technology*. **43**(14), 6839–6845 (2025).
115. N. Zhao, Y. Liu, M. Li, J. Li, J. Peng, L. Yang, N. Dai, H. Li, and J. Li, Mitigation of photodarkening effect in Yb-doped fiber through Na^+ ions doping, *Optics Express*. **25**(15), 18191–18196 (2017).
116. K. Schuster, S. Unger, C. Aichele, F. Lindner, S. Grimm, D. Litzkendorf, J. Kobelke, J. Bierlich, K. Wondraczek, and H. Bartelt, Material and technology trends in fiber optics, *Advanced Optical Technologies*. **3**(4), 447–468 (2014).
117. B. Meehan, A. R. Pietros, B. Topper, P. Karki, A. M. Rao, J. Liu, M. Urban, M. J. Jercinovic, R. Youngman, T. W. Hawkins, et al., Insights into draw-induced refractive index changes in intrinsically low nonlinearity MCVD preforms and optical fibers, *Optical Materials Express*. **15**(4), 661–673 (2025).
118. E. Strzelecki, D. Cohen, and L. Coldren, Investigation of tunable single frequency diode lasers for sensor applications, *Journal of Lightwave Technology*. **6**(10), 1610–1618 (2002).
119. A. Salhi, D. Barat, D. Romanini, Y. Rouillard, A. Ouvrard, R. Werner, J. Seufert, J. Koeth, A. Vicet, and A. Garnache, Single-frequency Sb-based distributed-feedback lasers emitting at $2.3\text{ }\mu\text{m}$ above room temperature for application in tunable diode laser absorption spectroscopy, *Applied Optics*. **45**(20), 4957–4965 (2006).
120. A. Jiménez, T. Milde, N. Staacke, C. Assmann, G. Carpintero, and J. Sacher, Narrow-line external cavity diode laser micro-packaging in the NIR and MIR spectral range, *Applied Physics B*. **123**(7), 207 (2017).
121. W. Loh and R. Laming, $1.55\text{ }\mu\text{m}$ phase-shifted distributed feedback fibre laser, *Electronics Letters*. **31**(17), 1440–1442 (1995).
122. S. Agger, J. H. Povlsen, and P. Varming, Single-frequency thulium-doped distributed-feedback fiber laser, *Optics Letters*. **29**(13), 1503–1505 (2004).

123. M. Bernier, V. Michaud-Belleau, S. Levasseur, V. Fortin, J. Genest, and R. Vallée, All-fiber DFB laser operating at 2.8 μ m, *Optics Letters*. **40**(1), 81–84 (2015).
124. Z. Xie, C. Shi, Q. Sheng, S. Fu, W. Shi, and J. Yao, A single-frequency 1064-nm Yb³⁺-doped fiber laser tandem-pumped at 1018 nm, *Optics Communications*. **461**, 125262 (2020).
125. S. Fu, X. Zhu, J. Zong, R. A. Norwood, and N. Peyghambarian, Diode-pumped 1.15 W linearly polarized single-frequency Yb³⁺-doped phosphate fiber laser, *Optics Express*. **29**(19), 30637–30643 (2021).
126. Y. Tao, S. Zhang, M. Jiang, C. Li, P. Zhou, and Z. Jiang, High power and high efficiency single-frequency 1030 nm DFB fiber laser, *Optics & Laser Technology*. **145**, 107519 (2022).
127. J. Zhang, Q. Sheng, L. Zhang, C. Shi, S. Sun, W. Shi, and J. Yao, 2.56 W Single-Frequency All-Fiber Oscillator at 1720 nm, *Advanced Photonics Research*. **3**(2), 2100256 (2022).
128. Y. Li, X. Deng, S. Fu, Q. Sheng, C. Shi, J. Zhang, L. Zhang, W. Shi, and J. Yao, High-power, high-efficiency single-frequency DBR fiber laser at 1064 nm based on Yb³⁺-doped silica fiber, *Optics Letters*. **48**(3), 598–601 (2023).
129. T. J. Kane, A. C. Nilsson, and R. L. Byer, Frequency stability and offset locking of a laser-diode-pumped Nd: YAG monolithic nonplanar ring oscillator, *Optics Letters*. **12**(3), 175–177 (1987).
130. C. Dixneuf, G. Guiraud, Y.-V. Bardin, Q. Rosa, M. Goeppner, A. Hilico, C. Pierre, J. Boulet, N. Traynor, and G. Santarelli, Ultra-low intensity noise, all fiber 365 W linearly polarized single frequency laser at 1064 nm, *Optics Express*. **28**(8), 10960–10969 (2020).
131. W. Lai, P. Ma, W. Liu, L. Huang, C. Li, Y. Ma, and P. Zhou, 550 W single frequency fiber amplifiers emitting at 1030 nm based on a tapered Yb-doped fiber, *Optics Express*. **28**(14), 20908–20919 (2020).
132. C. Shi, X. Deng, S. Fu, Q. Sheng, P. Jiang, Z. Shi, Y. Li, W. Shi, and J. Yao, 700 W single-frequency all-fiber amplifier at 1064 nm with kHz-level spectral linewidth, *Frontiers in Physics*. **10**, 982900 (2022).
133. R. W. Drever, J. L. Hall, F. V. Kowalski, J. Hough, G. Ford, A. Munley, and H. Ward, Laser phase and frequency stabilization using an optical resonator, *Applied Physics B*. **31**(2), 97–105 (1983).
134. C. Salomon, D. Hils, and J. Hall, Laser stabilization at the millihertz level, *Journal of the Optical Society of America B*. **5**(8), 1576–1587 (1988).
135. H. Lee, M.-G. Suh, T. Chen, J. Li, S. A. Diddams, and K. J. Vahala, Spiral resonators for on-chip laser frequency stabilization, *Nature Communications*. **4**(1), 2468 (2013).
136. S. Hirata, T. Akatsuka, Y. Ohtake, and A. Morinaga, Sub-hertz-linewidth diode laser stabilized to an ultralow-drift high-finesse optical cavity, *Applied Physics Express*. **7**(2), 022705 (2014).
137. W. Liang, V. Ilchenko, D. Eliyahu, A. Savchenkov, A. Matsko, D. Seidel, and L. Maleki, Ultralow noise miniature external cavity semiconductor laser, *Nature Communications*. **6**(1), 7371 (2015).
138. P. A. Morton and M. J. Morton, High-power, ultra-low noise hybrid lasers

for microwave photonics and optical sensing, *Journal of Lightwave Technology*. **36**(21), 5048–5057 (2018).

- 139. W. Jin, Q.-F. Yang, L. Chang, B. Shen, H. Wang, M. A. Leal, L. Wu, M. Gao, A. Feshali, M. Paniccia, et al., Hertz-linewidth semiconductor lasers using CMOS-ready ultra-high-Q microresonators, *Nature Photonics*. **15**(5), 346–353 (2021).
- 140. X. Zhang, K. Jia, S. Cheng, Y. Shi, S.-N. Zhu, and Z. Xie, Narrow-linewidth self-injection locking 1 μm laser using a fiber Fabry–Perot resonator, *Journal of the Optical Society of America B*. **42**(5), 1160–1163 (2025).
- 141. L. Rumbaugh Fiber Lasers and Amplifiers Design Toolbox, MATLAB Central File Exchange. (2013). <https://uk.mathworks.com/matlabcentral/fileexchange/42122-fiber-lasers-and-amplifiers-design-toolbox>.
- 142. B. Samson and G. Frith. Diode pump requirements for high power fiber lasers. In *International Congress on Applications of Lasers & Electro-Optics*, vol. 2007, p. 501 (2007).
- 143. E. Zucker, D. Zou, L. Zavala, H. Yu, P. Yalamanchili, L. Xu, H. Xu, D. Venables, J. Skidmore, V. Rossin, et al. Advancements in laser diode chip and packaging technologies for application in kW-class fiber laser pumping. In *High-Power Diode Laser Technology and Applications XII*, vol. 8965, pp. 38–51 (2014).
- 144. V. Gapontsev, N. Moshegov, I. Berezin, A. Komissarov, P. Trubenko, D. Miftakhutdinov, I. Berishev, V. Chuyanov, O. Raisky, and A. Ovtchinnikov. Highly-efficient high-power pumps for fiber lasers. In *High-Power Diode Laser Technology XV*, vol. 10086, pp. 16–25 (2017).
- 145. I. Berishev, A. Komissarov, N. Moshegov, P. Trubenko, L. Wright, A. Berezin, S. Todorov, and A. Ovtchinnikov. AlGaInAs/GaAs record high-power conversion efficiency and record high-brightness coolerless 915-nm multimode pumps. In *Novel In-Plane Semiconductor Lasers IV*, vol. 5738, pp. 25–32 (2005).
- 146. M. Kanskar, T. Earles, T. Goodnough, E. Stiers, D. Botez, and L. Mawst, 73% CW power conversion efficiency at 50 W from 970 nm diode laser bars, *Electronics Letters*. **41**(5), 245–247 (2005).
- 147. B. Volodin, S. Dolgy, E. Melnik, E. Downs, J. Shaw, and V. Ban, Wavelength stabilization and spectrum narrowing of high-power multimode laser diodes and arrays by use of volume Bragg gratings, *Optics Letters*. **29**(16), 1891–1893 (2004).
- 148. L. Talbot, S. Pelletier-Ouellet, F. Trépanier, and M. Bernier, Wavelength stabilization of high-power laser diodes using Bragg gratings inscribed in their highly multimode fiber pigtails, *Optics Letters*. **47**(3), 633–636 (2022).
- 149. W. Jiang, C. Yang, Q. Zhao, Q. Gu, J. Huang, K. Jiang, K. Zhou, Z. Feng, Z. Yang, and S. Xu. 650 W all-fiber single-frequency polarization-maintaining fiber amplifier based on hybrid wavelength pumping and tapered Yb-doped fibers. In *Photonics*, vol. 9, p. 518 (2022).
- 150. X. Chen, Y. Yang, M. Gong, P. Su, and J. Ma, 915 nm pumping kilowatt fiber oscillator with high optical-to-optical efficiency, *Scientific Reports*. **14**(1), 26331 (2024).

151. P. Zhou, H. Xiao, J. Leng, J. Xu, Z. Chen, H. Zhang, and Z. Liu, High-power fiber lasers based on tandem pumping, *Journal of the Optical Society of America B*. **34**(3), A29–A36 (2017).
152. P. Ma, H. Xiao, D. Meng, W. Liu, R. Tao, J. Leng, Y. Ma, R. Su, P. Zhou, and Z. Liu, High power all-fiberized and narrow-bandwidth MOPA system by tandem pumping strategy for thermally induced mode instability suppression, *High Power Laser Science and Engineering*. **6**, e57 (2018).
153. P. Baer, P. Cebeci, M. Reiter, F. Bontke, M. Giesberts, and H.-D. Hoffmann, Ultra-low-noise, single-frequency, all-PM Thulium-and Holmium-doped Fiber Amplifiers at 1950 nm and 2090 nm for third-generation Gravitational Wave Detectors, *IEEE Photonics Journal*. **16**(1), 1–9 (2024).
154. L. V. Kotov, V. Temyanko, M. M. Bubnov, D. S. Lipatov, A. S. Lobanov, A. Abramov, S. S. Aleshkina, A. N. Guryanov, and M. E. Likhachev, High-energy single-frequency core-pumped Er-doped fiber amplifiers, *Journal of Lightwave Technology*. **41**(5), 1526–1532 (2022).
155. O. d. Varona, M. Steinke, J. Neumann, and D. Kracht, All-fiber, single-frequency, and single-mode Er³⁺:Yb³⁺ fiber amplifier at 1556 nm core-pumped at 1018 nm, *Optics Letters*. **43**(11), 2632–2635 (2018).
156. A. Braglia, A. Califano, Y. Liu, and G. Perrone, Architectures and components for high power CW fiber lasers, *International Journal of Modern Physics B*. **28**(12), 1442001 (2014).
157. M. N. Zervas, High power ytterbium-doped fiber lasers—fundamentals and applications, *International Journal of Modern Physics B*. **28**(12), 1442009 (2014).
158. Z. Li, Z. Huang, X. Xiang, X. Liang, H. Lin, S. Xu, Z. Yang, J. Wang, and F. Jing, Experimental demonstration of transverse mode instability enhancement by a counter-pumped scheme in a 2 kW all-fiberized laser, *Photonics Research*. **5**(2), 77–81 (2017).
159. D. Stachowiak. High-power passive fiber components for all-fiber lasers and amplifiers application—design and fabrication. In *Photonics*, vol. 5, p. 38 (2018).
160. Y. Liu, K. Liu, Y. Yang, M. Liu, B. He, and J. Zhou, High power pump and signal combiner for backward pumping structure with two different fused fiber bundle designs by means of pretapered pump fibers, *Optics Express*. **29**(9), 13344–13358 (2021).
161. D. Majumder, S. Das Chowdhury, and A. Pal, Design and fabrication of a tapered fiber bundle for a pump combiner with a uniform splicing region, *Journal of the Optical Society of America B*. **39**(7), 1871–1878 (2022).
162. Y. Tao, M. Jiang, L. Liu, C. Li, P. Zhou, and Z. Jiang, Over 250 W low noise core-pumped single-frequency all-fiber amplifier, *Optics Express*. **31**(6), 10586–10595 (2023).
163. C. Jauregui, S. Böhme, G. Wenetiadis, J. Limpert, and A. Tünnermann, Side-pump combiner for all-fiber monolithic fiber lasers and amplifiers, *Journal of the Optical Society of America B*. **27**(5), 1011–1015 (2010).
164. S. Magnan-Saucier, S. Duval, C. Matte-Breton, Y. O. Aydin, V. Fortin, S. LaRochelle, M. Bernier, and R. Vallée, Fuseless side-pump combiner for

efficient fluoride-based double-clad fiber pumping, *Optics Letters*. **45**(20), 5828–5831 (2020).

165. E. Brockmüller, F. Kranert, R. Lachmayer, J. Neumann, and D. Kracht. Side-fused signal-pump combiner for triple clad fibers. In *Fiber Lasers XXII: Technology and Systems*, vol. 13342, pp. 132–138 (2025).
166. E. Shcherbakov, V. Fomin, A. Abramov, A. Ferin, D. Mochalov, and V. P. Gapontsev. Industrial grade 100 kW power CW fiber laser. In *Advanced Solid State Lasers*, pp. ATh4A-2 (2013).
167. J. Sun, L. Liu, L. Han, Q. Zhu, X. Shen, and K. Yang, 100 kW ultra high power fiber laser, *Optics Continuum*. **1**(9), 1932–1938 (2022).
168. Y. Jeong, J. Nilsson, J. Sahu, D. Soh, C. Alegria, P. Dupriez, C. Codemard, D. Payne, R. Horley, L. Hickey, et al., Single-frequency, single-mode, plane-polarized ytterbium-doped fiber master oscillator power amplifier source with 264 W of output power, *Optics Letters*. **30**(5), 459–461 (2005).
169. C. Robin, I. Dajani, and B. Pulford, Modal instability-suppressing, single-frequency photonic crystal fiber amplifier with 811 W output power, *Optics Letters*. **39**(3), 666–669 (2014).
170. F. Beier, C. Hupel, S. Kuhn, S. Hein, J. Nold, F. Proske, B. Sattler, A. Liem, C. Jauregui, J. Limpert, et al., Single mode 4.3 kW output power from a diode-pumped Yb-doped fiber amplifier, *Optics Express*. **25**(13), 14892–14899 (2017).
171. D. L. Smith, O. Henderson-Sapir, J. Singh, S. Wei, L. V. Nguyen, H. Ebendorff-Heidepriem, S. C. Warren-Smith, and D. J. Ottaway. Wavefront Shaping for Near-Diffraction Limited Multimode Output in a Record Peak Power, Single-Frequency, 1.5 μ m Fiber Amplifier. In *2025 Conference on Lasers and Electro-Optics (CLEO)*, pp. 1–2 (2025).
172. G. P. Agrawal. Nonlinear fiber optics. In *Nonlinear Science at the Dawn of the 21st Century*, pp. 195–211. Springer (2000).
173. B. J. Eggleton, C. G. Poulton, and R. Pant, Inducing and harnessing stimulated Brillouin scattering in photonic integrated circuits, *Advances in Optics and Photonics*. **5**(4), 536–587 (2013).
174. K. Wisal, C.-W. Chen, and S. Warren-Smith Codes for “Mitigating stimulated Brillouin scattering in multimode fibers with focused output via wavefront shaping,” *Zenodo*. DOI: 10.5281/zenodo.8357385 (2023). <https://github.com/kabishhwisal/SBS-optimization>.
175. S. Rothe, C.-W. Chen, P. Ahmadi, K. Lee, K. Wisal, M. Ercan, N. Vigne, A. D. Stone, and H. Cao, Wavefront shaping enables high-power multimode fiber amplifier with output focus, *Science*. **390**(6769), 173–177 (2025).
176. R. W. Boyd, K. Rzaewski, and P. Narum, Noise initiation of stimulated brillouin scattering, *Physical review A*. **42**(9), 5514 (1990).
177. A. L. Gaeta and R. W. Boyd, Stochastic dynamics of stimulated Brillouin scattering in an optical fiber, *Physical Review A*. **44**(5), 3205 (1991).
178. S. Gray, A. Liu, D. T. Walton, J. Wang, M.-J. Li, X. Chen, A. B. Ruffin, J. A. DeMeritt, and L. A. Zenteno, 502 Watt, single transverse mode, narrow linewidth, bidirectionally pumped Yb-doped fiber amplifier, *Optics Express*. **15**(25), 17044–17050 (2007).

179. S. Hochheim, M. Steinke, P. Wessels, O. De Varona, J. Koponen, T. Lowder, S. Novotny, J. Neumann, and D. Kracht, Single-frequency chirally coupled-core all-fiber amplifier with 100 W in a linearly polarized TEM00 mode, *Optics Letters*. **45**(4), 939–942 (2020).
180. K. Kruska, P. Weßels, J. Neumann, and D. Kracht. Power scaling of single-frequency Yb³⁺ fiber amplifiers with highly absorbing standard LMA fibers. In *Fiber Lasers XXII: Technology and Systems*, vol. 13342, p. 1334214 (2025).
181. T. Matniyaz, S. P. Bingham, M. T. Kalichevsky-Dong, T. W. Hawkins, B. Pulford, and L. Dong, High-power single-frequency single-mode all-solid photonic bandgap fiber laser with kHz linewidth, *Optics Letters*. **47**(2), 377–380 (2022).
182. A. Liem, J. Limpert, H. Zellmer, and A. Tünnermann, 100-W single-frequency master-oscillator fiber power amplifier, *Optics Letters*. **28**(17), 1537–1539 (2003).
183. X. Wang, P. Zhou, H. Xiao, Y. Ma, X. Xu, and Z. Liu, 310 W single-frequency all-fiber laser in master oscillator power amplification configuration, *Laser Physics Letters*. **9**(8), 591 (2012).
184. P. Ma, P. Zhou, Y. Ma, R. Su, X. Xu, and Z. Liu, Single-frequency 332 W, linearly polarized Yb-doped all-fiber amplifier with near diffraction-limited beam quality, *Applied Optics*. **52**(20), 4854–4857 (2013).
185. I. Dajani, C. Vergien, C. Robin, and C. Zeringue, Experimental and theoretical investigations of photonic crystal fiber amplifier with 260 W output, *Optics Express*. **17**(26), 24317–24333 (2009).
186. C. Robin and I. Dajani, Acoustically segmented photonic crystal fiber for single-frequency high-power laser applications, *Optics Letters*. **36**(14), 2641–2643 (2011).
187. J. Limpert, F. Stutzki, F. Jansen, H.-J. Otto, T. Eidam, C. Jauregui, and A. Tünnermann, Yb-doped large-pitch fibres: effective single-mode operation based on higher-order mode delocalisation, *Light: Science & Applications*. **1**(4), e8–e8 (2012).
188. B. Pulford, T. Ehrenreich, R. Holten, F. Kong, T. W. Hawkins, L. Dong, and I. Dajani, 400-W near diffraction-limited single-frequency all-solid photonic bandgap fiber amplifier, *Optics Letters*. **40**(10), 2297–2300 (2015).
189. C. Zhu, I.-N. Hu, X. Ma, and A. Galvanauskas. Single-frequency and single-transverse mode Yb-doped CCC fiber MOPA with robust polarization SBS-free 511W output. In *Advanced Solid-State Photonics*, p. AMC5 (2011).
190. L. Dong, X. Peng, and J. Li, Leakage channel optical fibers with large effective area, *Journal of the Optical Society of America B*. **24**(8), 1689–1697 (2007).
191. Y. Cheng, Q. Yang, Y. Zhu, D. Wu, C. Yu, Y. Sun, Y. Chen, Q. Zhou, X. Wang, F. Yu, et al., Design and fabrication of all-solid anti-resonant silicate fibers for Yb ASE suppression in Er/Yb fiber amplifier, *Optics Express*. **32**(19), 33962–33973 (2024).
192. J. Sousa and O. Okhotnikov, Multimode Er-doped fiber for single-transverse-mode amplification, *Applied Physics Letters*. **74**(11), 1528–1530

(1999).

193. M. A. Cooper, S. Gausmann, J. E. Antonio-Lopez, A. Schülzgen, and R. A. Correa. Confined doping LMA fibers for high power single frequency lasers. In *Fiber Lasers XIX: Technology and Systems*, vol. 11981, pp. 23–29 (2022).
194. W. Li, Z. Yan, S. Ren, Y. Deng, Y. Chen, P. Ma, W. Liu, L. Huang, Z. Pan, P. Zhou, et al., Confined-doped active fiber enabled all-fiber high-power single-frequency laser, *Optics Letters*. **47**(19), 5024–5027 (2022).
195. K. Kruska, P. Booker, P. Weßels, J. Neumann, and D. Kracht. High-power single-frequency depressed-cladding, confined-doping Yb³⁺ fiber amplifier. In *Fiber Lasers XXI: Technology and Systems*, vol. 12865, pp. 185–190 (2024).
196. A. Trikshev, A. Kurkov, V. Tsvetkov, S. Filitova, J. Kertulla, V. Filippov, Y. K. Chamorovskiy, and O. G. Okhotnikov, A 160 W single-frequency laser based on an active tapered double-clad fiber amplifier, *Laser Physics Letters*. **10**(6), 065101 (2013).
197. C. Pierre, G. Guiraud, J.-P. Yehouessi, G. Santarelli, J. Boullet, N. Traynor, and C. VINCONT. 200-W single frequency laser based on short active double clad tapered fiber. In *Fiber Lasers XV: Technology and Systems*, vol. 10512, pp. 403–403 (2018).
198. K. Shiraki, M. Ohashi, and M. Tateda, Suppression of stimulated Brillouin scattering in a fibre by changing the core radius, *Electronics letters*. **31**(8), 668–669 (1995).
199. S. Kholaif, C. Jauregui, J. Nold, N. Haarlamert, S. Kuhn, T. Schreiber, and J. Limpert, Influence of core size on the transverse mode instability threshold of fiber amplifiers, *Optics Express*. **33**(26), 54245–54256 (2025).
200. P. D. Dragic, J. Ballato, and T. W. Hawkins. Low-nonlinearity optical fibers and their applications. In *Specialty Optical Fibers*, pp. 303–344. Elsevier (2024).
201. A. Melloni, M. Frasca, A. Garavaglia, A. Tonini, and M. Martinelli, Direct measurement of electrostriction in optical fibers, *Optics Letters*. **23**(9), 691–693 (1998).
202. P. D. Dragic, Brillouin Gain Reduction Via B₂O₃ Doping, *Journal of Lightwave Technology*. **29**(7), 967–973 (2011).
203. P. D. Dragic, J. Ballato, S. Morris, and T. Hawkins, Pockels' coefficients of alumina in aluminosilicate optical fiber, *Journal of the Optical Society of America B*. **30**(2), 244–250 (2013).
204. P. D. Dragic, J. Ballato, S. Morris, and T. Hawkins, The Brillouin gain coefficient of Yb-doped aluminosilicate glass optical fibers, *Optical Materials*. **35**(9), 1627–1632 (2013).
205. P. Dragic, C. Kucera, J. Furtick, J. Guerrier, T. Hawkins, and J. Ballato, Brillouin spectroscopy of a novel baria-doped silica glass optical fiber, *Optics Express*. **21**(9), 10924–10941 (2013).
206. M. Cavillon, J. Furtick, C. J. Kucera, C. Ryan, M. Tuggle, M. Jones, T. W. Hawkins, P. Dragic, and J. Ballato, Brillouin properties of a novel strontium aluminosilicate glass optical fiber, *Journal of Lightwave Technology*. **34**(6), 1435–1441 (2016).

207. A. Bertholds and R. Dandliker, Determination of the individual strain-optic coefficients in single-mode optical fibres, *Journal of Lightwave Technology*. **6**(1), 17–20 (2002).
208. P.-C. Law, Y.-S. Liu, A. Croteau, and P. D. Dragic, Acoustic coefficients of P_2O_5 -doped silica fiber: acoustic velocity, acoustic attenuation, and thermo-acoustic coefficient, *Optical Materials Express*. **1**(4), 686–699 (2011).
209. N. Yu, T. W. Hawkins, T.-V. Bui, M. Cavillon, J. Ballato, and P. D. Dragic, $AlPO_4$ in silica glass optical fibers: deduction of additional material properties, *IEEE Photonics Journal*. **11**(5), 1–13 (2019).
210. P. Dragic, P.-C. Law, J. Ballato, T. Hawkins, and P. Foy, Brillouin spectroscopy of YAG-derived optical fibers, *Optics Express*. **18**(10), 10055–10067 (2010).
211. P. Dragic, T. Hawkins, P. Foy, S. Morris, and J. Ballato, Sapphire-derived all-glass optical fibres, *Nature Photonics*. **6**(9), 627–633 (2012).
212. K. Wisal, S. C. Warren-Smith, C.-W. Chen, H. Cao, and A. D. Stone, Theory of stimulated Brillouin scattering in fibers for highly multimode excitations, *Physical Review X*. **14**(3), 031053 (2024).
213. T. Horiguchi, K. Shimizu, T. Kurashima, M. Tateda, and Y. Koyamada, Development of a distributed sensing technique using Brillouin scattering, *Journal of Lightwave Technology*. **13**(7), 1296–1302 (2002).
214. Y. Imai and N. Shimada, Dependence of stimulated Brillouin scattering on temperature distribution in polarization-maintaining fibers, *IEEE photonics technology letters*. **5**(11), 1335–1337 (1993).
215. N. Yoshizawa and T. Imai, Stimulated Brillouin scattering suppression by means of applying strain distribution to fiber with cabling, *Journal of Lightwave Technology*. **11**(10), 1518–1522 (1993).
216. J. C. Boggio, J. Marconi, and H. Fragnito, Experimental and numerical investigation of the SBS-threshold increase in an optical fiber by applying strain distributions, *Journal of Lightwave Technology*. **23**(11), 3808–3814 (2005).
217. I. Dajani, C. Zeringue, C. Lu, C. Vergien, L. Henry, and C. Robin, Stimulated Brillouin scattering suppression through laser gain competition: scalability to high power, *Optics Letters*. **35**(18), 3114–3116 (2010).
218. L. Zhang, S. Cui, C. Liu, J. Zhou, and Y. Feng, 170 W, single-frequency, single-mode, linearly-polarized, Yb-doped all-fiber amplifier, *Optics Express*. **21**(5), 5456–5462 (2013).
219. Y. Jeong, J. Nilsson, J. K. Sahu, D. N. Payne, R. Horley, L. Hickey, and P. Turner, Power scaling of single-frequency ytterbium-doped fiber master-oscillator power-amplifier sources up to 500 W, *IEEE Journal of Selected Topics in Quantum Electronics*. **13**(3), 546–551 (2007).
220. C. Zeringue, C. Vergien, and I. Dajani, Pump-limited, 203 W, single-frequency monolithic fiber amplifier based on laser gain competition, *Optics Letters*. **36**(5), 618–620 (2011).
221. T. Theeg, C. Ottenhues, H. Sayinc, J. Neumann, and D. Kracht, Core-pumped single-frequency fiber amplifier with an output power of 158 W, *Optics Letters*. **41**(1), 9–12 (2015).

222. T. Theeg, H. Sayinc, J. Neumann, and D. Kracht, All-fiber counter-propagation pumped single frequency amplifier stage with 300-W output power, *IEEE Photonics Technology Letters*. **24**(20), 1864–1867 (2012).

223. J. Hansryd, F. Dross, M. Westlund, P. Andrekson, and S. Knudsen, Increase of the SBS threshold in a short highly nonlinear fiber by applying a temperature distribution, *Journal of Lightwave Technology*. **19**(11), 1691 (2001).

224. L. Huang, H. Wu, R. Li, L. Li, P. Ma, X. Wang, J. Leng, and P. Zhou, 414 W near-diffraction-limited all-fiberized single-frequency polarization-maintained fiber amplifier, *Optics Letters*. **42**(1), 1–4 (2016).

225. E. Balliu. *Power Scaling of Highly Compact Single-Frequency Yb-Doped Fiber Amplifiers*. PhD thesis, Mid Sweden University (2022).

226. J. Montoya, C. Hwang, D. Martz, C. Aleshire, T. Fan, and D. J. Ripin, Photonic lantern kW-class fiber amplifier, *Optics Express*. **25**(22), 27543–27550 (2017).

227. R. S. Williamson III, Laser coherence control using homogeneous linewidth broadening (2007). US Patent 7,280,568.

228. C. Zeringue, I. Dajani, S. Naderi, G. T. Moore, and C. Robin, A theoretical study of transient stimulated Brillouin scattering in optical fibers seeded with phase-modulated light, *Optics Express*. **20**(19), 21196–21213 (2012).

229. B. Anderson, A. Flores, R. Holten, and I. Dajani, Comparison of phase modulation schemes for coherently combined fiber amplifiers, *Optics Express*. **23**(21), 27046–27060 (2015).

230. A. Flores, C. Lu, C. Robin, S. Naderi, C. Vergien, and I. Dajani, Experimental and theoretical studies of phase modulation in Yb-doped fiber amplifiers. In *Laser Technology for Defense and Security VIII*, vol. 8381, pp. 271–278 (2012).

231. A. Flores, C. Robin, A. Lanari, and I. Dajani, Pseudo-random binary sequence phase modulation for narrow linewidth, kilowatt, monolithic fiber amplifiers, *Optics Express*. **22**(15), 17735–17744 (2014).

232. B. Ward, C. Robin, and I. Dajani, Origin of thermal modal instabilities in large mode area fiber amplifiers, *Optics Express*. **20**(10), 11407–11422 (2012).

233. K. R. Hansen, T. T. Alkeskjold, J. Broeng, and J. Lægsgaard, Theoretical analysis of mode instability in high-power fiber amplifiers, *Optics Express*. **21**(2), 1944–1971 (2013).

234. S. Naderi, I. Dajani, T. Madden, and C. Robin, Investigations of modal instabilities in fiber amplifiers through detailed numerical simulations, *Optics Express*. **21**(13), 16111–16129 (2013).

235. L. Dong, Stimulated thermal rayleigh scattering in optical fibers, *Optics Express*. **21**(3), 2642–2656 (2013).

236. F. Kong, J. Xue, R. H. Stolen, and L. Dong, Direct experimental observation of stimulated thermal Rayleigh scattering with polarization modes in a fiber amplifier, *Optica*. **3**(9), 975–978 (2016).

237. C. Jauregui, Y. Tu, S. Kholaif, F. Möller, G. Palma-Vega, N. Haarlammert, T. Walbaum, T. Schreiber, and J. Limpert, Recent developments in the

understanding and passive mitigation of transverse mode instability, *Optical Fiber Technology*. **96**, 104496 (2026).

- 238. C.-W. Chen, K. Wisal, Y. Eliezer, A. D. Stone, and H. Cao, Suppressing transverse mode instability through multimode excitation in a fiber amplifier, *Proceedings of the National Academy of Sciences*. **120**(22), e2217735120 (2023).
- 239. C.-W. Chen, Y. Eliezer, and K. Wisal Spacetime symmetry mapping in a dissipative nonlinear multimode waveguide amplifier, *GitHub*. (2024). <https://github.com/joe851642001/MWAT>.
- 240. C.-W. Chen, K. Wisal, M. Fink, A. D. Stone, and H. Cao, Output control of dissipative nonlinear multimode amplifiers using spacetime symmetry mapping, *Nature Physics*. pp. 1–7 (2025).
- 241. C. Stihler, C. Jauregui, S. E. Kholoif, and J. Limpert, Intensity noise as a driver for transverse mode instability in fiber amplifiers, *PhotonX*. **1**(1), 8 (2020).
- 242. T. Eidam, C. Wirth, C. Jauregui, F. Stutzki, F. Jansen, H.-J. Otto, O. Schmidt, T. Schreiber, J. Limpert, and A. Tünnermann, Experimental observations of the threshold-like onset of mode instabilities in high power fiber amplifiers, *Optics Express*. **19**(14), 13218–13224 (2011).
- 243. S. L. Christensen, M. M. Johansen, M. Michieletto, M. Triches, M. D. Maack, and J. Lægsgaard, Experimental investigations of seeding mechanisms of TMI in rod fiber amplifier using spatially and temporally resolved imaging, *Optics Express*. **28**(18), 26690–26705 (2020).
- 244. H.-J. Otto, F. Stutzki, F. Jansen, T. Eidam, C. Jauregui, J. Limpert, and A. Tünnermann, Temporal dynamics of mode instabilities in high-power fiber lasers and amplifiers, *Optics Express*. **20**(14), 15710–15722 (2012).
- 245. M. M. Johansen, M. Laurila, M. D. Maack, D. Noordgraaf, C. Jakobsen, T. T. Alkeskjold, and J. Lægsgaard, Frequency resolved transverse mode instability in rod fiber amplifiers, *Optics Express*. **21**(19), 21847–21856 (2013).
- 246. J. P. Koplow, D. A. Kliner, and L. Goldberg, Single-mode operation of a coiled multimode fiber amplifier, *Optics Letters*. **25**(7), 442–444 (2000).
- 247. R. Tao, R. Su, P. Ma, X. Wang, and P. Zhou, Suppressing mode instabilities by optimizing the fiber coiling methods, *Laser Physics Letters*. **14**(2), 025101 (2016).
- 248. F. Stutzki, F. Jansen, H.-J. Otto, C. Jauregui, J. Limpert, and A. Tünnermann, Designing advanced very-large-mode-area fibers for power scaling of fiber-laser systems, *Optica*. **1**(4), 233–242 (2014).
- 249. T. Eidam, S. Hädrich, F. Jansen, F. Stutzki, J. Rothhardt, H. Carstens, C. Jauregui, J. Limpert, and A. Tünnermann, Preferential gain photonic-crystal fiber for mode stabilization at high average powers, *Optics Express*. **19**(9), 8656–8661 (2011).
- 250. W. Li, S. Ren, Y. Deng, Y. Chen, Y. Lu, W. Liu, P. Ma, Z. Pan, Z. Chen, L. Si, et al., Investigation of the confined-doped fiber on single-mode operating and power scaling in all-fiber single-frequency amplifiers, *Frontiers in Physics*. **10**, 1016047 (2022).
- 251. D. C. Brown and H. J. Hoffman, Thermal, stress, and thermo-optic effects in

high average power double-clad silica fiber lasers, *IEEE Journal of Quantum Electronics*. **37**(2), 207–217 (2002).

- 252. L. Dong, Transverse mode instability considering bend loss and heat load, *Optics Express*. **31**(12), 20480–20488 (2023).
- 253. M. Cavillon, P. Dragic, and J. Ballato, Additivity of the coefficient of thermal expansion in silicate optical fibers, *Optics Letters*. **42**(18), 3650–3653 (2017).
- 254. M. Laurila, M. M. Jørgensen, K. R. Hansen, T. T. Alkeskjold, J. Broeng, and J. Lægsgaard, Distributed mode filtering rod fiber amplifier delivering 292W with improved mode stability, *Optics Express*. **20**(5), 5742–5753 (2012).
- 255. F. Jansen, F. Stutzki, H.-J. Otto, C. Jauregui, J. Limpert, and A. Tünnermann, High-power thermally guiding index-antiguide-core fibers, *Opt. Lett.* **38**(4), 510–512 (Feb, 2013).
- 256. A. V. Smith and J. J. Smith, Increasing mode instability thresholds of fiber amplifiers by gain saturation, *Optics Express*. **21**(13), 15168–15182 (2013).
- 257. K. R. Hansen and J. Lægsgaard, Impact of gain saturation on the mode instability threshold in high-power fiber amplifiers, *Optics Express*. **22**(9), 11267–11278 (2014).
- 258. B. Ward, Theory and modeling of photodarkening-induced quasi static degradation in fiber amplifiers, *Optics Express*. **24**(4), 3488–3501 (2016).
- 259. L. Dong, Accurate modeling of transverse mode instability in fiber amplifiers, *Journal of Lightwave Technology*. **40**(14), 4795–4803 (2022).
- 260. K. Wisal, C.-W. Chen, H. Cao, and A. D. Stone, Theory of transverse mode instability in fiber amplifiers with multimode excitations, *APL Photonics*. **9**(6) (2024).
- 261. C. Shi, S. Fu, X. Deng, Q. Sheng, Y. Xu, Q. Fang, S. Sun, J. Zhang, W. Shi, and J. Yao, 435 W single-frequency all-fiber amplifier at 1064 nm based on cascaded hybrid active fibers, *Optics Communications*. **502**, 127428 (2022).
- 262. C. Shi, H. Tian, S. Fu, Q. Sheng, Z. Shi, P. Jiang, W. Shi, and J. Yao, High-energy single-frequency pulsed fiber MOPA at 1064 nm based on a hybrid active-fiber, *Optics Express*. **30**(9), 15575–15582 (2022).
- 263. C. Ren, Y. Hu, Y. Song, H. Wang, J. Guo, F. Wang, and D. Shen, 425-W kilohertz-linewidth single-frequency Tm-fiber MOPA enabled by distributed cladding-pumping, *Optics Express*. **33**(17), 36358–36367 (2025).
- 264. I. Dajani, C. Zeringue, and T. M. Shay, Investigation of nonlinear effects in multitone-driven narrow-linewidth high-power amplifiers, *IEEE Journal of Selected Topics in Quantum Electronics*. **15**(2), 406–414 (2009).
- 265. H.-J. Otto, C. Jauregui, F. Stutzki, F. Jansen, J. Limpert, and A. Tünnermann, Controlling mode instabilities by dynamic mode excitation with an acousto-optic deflector, *Optics Express*. **21**(14), 17285–17298 (2013).
- 266. C. Jauregui, C. Stihler, A. Tünnermann, and J. Limpert, Pump-modulation-induced beam stabilization in high-power fiber laser systems above the mode instability threshold, *Optics Express*. **26**(8), 10691–10704 (2018).

267. W. Kim, C. Florea, C. Baker, D. Gibson, L. Shaw, S. Bowman, S. O'Connor, G. Villalobos, S. Bayya, I. Aggarwal, et al. Single crystal fibers for high power lasers. In *High-Power Lasers 2012: Technology and Systems*, vol. 8547, pp. 123–128 (2012).
268. M. Dubinskii, J. Zhang, V. Fromzel, Y. Chen, S. Yin, and C. Luo, Low-loss ‘crystalline-core/crystalline-clad’(C4) fibers for highly power scalable high efficiency fiber lasers, *Optics Express*. **26**(4), 5092–5101 (2018).
269. L. Dong, J. Ballato, and J. Kolis, Power scaling limits of diffraction-limited fiber amplifiers considering transverse mode instability, *Optics Express*. **31**(4), 6690–6703 (2023).
270. Z. Huang, B. Rao, Z. Wang, C. Gao, H. Xiao, B. Yi, Z. Chen, P. Ma, J. Zeng, D. Shi, et al., High-brightness multimode fiber laser amplifier, *arXiv preprint arXiv:2504.08261* (2025).
271. C.-W. Chen, L. V. Nguyen, K. Wisal, S. Wei, S. C. Warren-Smith, O. Henderson-Sapir, E. P. Schartner, P. Ahmadi, H. Ebendorff-Heidepriem, A. D. Stone, et al., Mitigating stimulated Brillouin scattering in multimode fibers with focused output via wavefront shaping, *Nature Communications*. **14**(1), 7343 (2023).
272. K. Wisal, C.-W. Chen, Z. Kuang, O. D. Miller, H. Cao, and A. D. Stone, Optimal input excitations for suppressing nonlinear instabilities in multimode fibers, *Optica*. **11**(12), 1663–1672 (2024).
273. F. Zhang, H. Xu, Y. Xing, S. Hou, Y. Chen, J. Li, N. Dai, H. Li, Y. Wang, and L. Liao, Bending diameter dependence of mode instabilities in multimode fiber amplifier, *Laser physics letters*. **16**(3), 035104 (2019).
274. Y. Wen, P. Wang, C. Shi, B. Yang, X. Xi, H. Zhang, and X. Wang, Experimental study on transverse mode instability characteristics of few-mode fiber laser amplifier under different bending conditions, *IEEE Photonics Journal*. **14**(4), 1–6 (2022).
275. R. Li, H. Li, H. Wu, H. Xiao, J. Leng, L. Huang, Z. Pan, and P. Zhou, Mitigation of TMI in an 8 kW tandem pumped fiber amplifier enabled by inter-mode gain competition mechanism through bending control, *Optics Express*. **31**(15), 24423–24436 (2023).
276. S. Rothe, K. Wisal, C.-W. Chen, M. Ercan, A. Jesacher, A. D. Stone, and H. Cao, Output beam shaping of a multimode fiber amplifier, *Optics Communications*. **577**, 131405 (2025).
277. B. Redding, S. M. Popoff, and H. Cao, All-fiber spectrometer based on speckle pattern reconstruction, *Optics Express*. **21**(5), 6584–6600 (2013).
278. R. Florentin, V. Kermene, J. Benoist, A. Desfarges-Berthelemot, D. Pagnoux, A. Barthélémy, and J.-P. Huignard, Shaping the light amplified in a multimode fiber, *Light: Science & Applications*. **6**(2), e16208–e16208 (2017).
279. R. Florentin, V. Kermene, A. Desfarges-Berthelemot, and A. Barthélémy, Shaping of amplified beam from a highly multimode Yb-doped fiber using transmission matrix, *Optics Express*. **27**(22), 32638–32648 (2019).
280. M. Hughes Fibre Mode Solver and Simulator, MATLAB Central File Exchange. (2020). <https://uk.mathworks.com/matlabcentral/>

fileexchange/77497-fibre-mode-solver-and-simulator.

281. N. Yu, J. Ballato, M. J. Digonnet, and P. D. Dragic, Optically managing thermal energy in high-power Yb-doped fiber lasers and amplifiers: a brief review, *Current Optics and Photonics*. **6**(6), 521–549 (2022).
282. S. R. Bowman, Lasers without internal heat generation, *IEEE Journal of Quantum Electronics*. **35**(1), 115–122 (2002).
283. S. R. Bowman, S. P. O'Connor, S. Biswal, N. J. Condon, and A. Rosenberg, Minimizing heat generation in solid-state lasers, *IEEE Journal of Quantum Electronics*. **46**(7), 1076–1085 (2010).
284. J. Knall, T. Boilard, M. Bernier, P.-B. Vigneron, N. Yu, P. Dragic, J. Ballato, and M. Digonnet, Radiation-balanced silica fiber laser, *Optica*. **8**(6), 830–833 (2021).
285. J. M. Knall, M. Engholm, T. Boilard, M. Bernier, and M. J. Digonnet, Radiation-balanced silica fiber amplifier, *Physical Review Letters*. **127**(1), 013903 (2021).
286. J. M. Knall and M. J. Digonnet, Design of high-power radiation-balanced silica fiber lasers with a doped core and cladding, *Journal of Lightwave Technology*. **39**(8), 2497–2504 (2021).
287. J. M. Knall and M. Esmaeelpour, Model of anti-Stokes fluorescence cooling in a single-mode optical fiber, *Journal of Lightwave Technology*. **36**(20), 4752–4760 (2018).
288. J. Knall, P.-B. Vigneron, M. Engholm, P. D. Dragic, N. Yu, J. Ballato, M. Bernier, and M. J. Digonnet, Laser cooling in a silica optical fiber at atmospheric pressure, *Optics Letters*. **45**(5), 1092–1095 (2020).
289. J. Knall, M. Engholm, J. Ballato, P. D. Dragic, N. Yu, and M. J. Digonnet, Experimental comparison of silica fibers for laser cooling, *Optics Letters*. **45**(14), 4020–4023 (2020).
290. C.-W. Chen, E. Balliu, B. Meehan, T. W. Hawkins, J. Ballato, P. D. Dragic, T. Boilard, M. Bernier, and M. J. Digonnet, Observation of anti-Stokes-fluorescence cooling in commercial Yb-doped silica fibers, *Applied Physics Letters*. **127**(14) (2025).
291. B. Meehan, A. R. Pietros, C.-W. Chen, T. W. Hawkins, M. Engholm, P. D. Dragic, M. J. Digonnet, and J. Ballato, Impact of Yb^{2+} on the anti-Stokes fluorescence cooling performance of Yb-doped silica fibers, *Optical Materials Express*. **14**(8), 2095–2111 (2024).
292. C.-W. Chen, B. Meehan, T. W. Hawkins, J. Ballato, P. D. Dragic, T. Boilard, M. Bernier, and M. J. Digonnet, Optical cooling of a Yb-doped alumino- Si_2O_5 phosphosilicate fiber in air by -250 mK, *Optics Letters*. **49**(16), 4501–4504 (2024).
293. E. Balliu, B. Meehan, M. A. Cahoon, T. W. Hawkins, J. Ballato, P. D. Dragic, T. Boilard, L. Talbot, M. Bernier, and M. J. Digonnet, High-efficiency radiation-balanced Yb-doped silica fiber laser with 200-mW output, *Optics Letters*. **49**(8), 2021–2024 (2024).
294. E. Balliu, B. Meehan, M. A. Cahoon, T. W. Hawkins, J. Ballato, P. D. Dragic, T. Boilard, L. Talbot, M. Bernier, and M. J. Digonnet, Single-mode radiation-balanced Yb-doped silica fiber laser and amplifier. In *Photonic*

Heat Engines: Science and Applications VI, vol. 12902, pp. 4–10 (2024).

- 295. C.-W. Chen, E. Balliu, B. Meehan, T. W. Hawkins, J. Ballato, P. D. Dragic, T. Boilard, M. Bernier, and M. J. Digonnet. Advancing athermal silica fiber lasers to watt-level power and beyond. In *Photonic Heat Engines: Science and Applications VII*, vol. 13379, p. 1337904 (2025).
- 296. C.-W. Chen, E. Balliu, B. Meehan, T. W. Hawkins, J. Ballato, P. D. Dragic, T. Boilard, M. Bernier, and M. J. Digonnet, Radiation-Balanced Fiber Amplifier with 600-mW Output *Under review*.
- 297. N. Yu, K. V. Desai, A. E. Mironov, M. Xiong, M. Cavillon, T. Hawkins, J. Ballato, J. G. Eden, and P. D. Dragic, Reduced quantum defect in a Yb-doped fiber laser by balanced dual-wavelength excitation, *Applied Physics Letters*. **119**(14) (2021).
- 298. N. Yu, M. Xiong, and P. D. Dragic, FDTD modeling of excitation-balanced, mJ-level pulse amplifiers in Yb-doped double-clad optical fibers, *Optics Express*. **31**(20), 32404–32421 (2023).
- 299. Y. Tao, Z. Mo, P. Kang, M. Jiang, C. Li, J. Leng, P. Zhou, and Z. Jiang. Experimental Study on Transverse Mode Instability of All-Fiber Single-Frequency Amplifier Based on Tapered Yb-Doped Fiber. In *Photonics*, vol. 11, p. 696 (2024).